

# Forming Disk Galaxies in $\Lambda$ CDM Simulations

F. Governato<sup>1,2</sup>, B. Willman<sup>3</sup>, L. Mayer<sup>4</sup>, A. Brooks<sup>1</sup>, G. Stinson<sup>1</sup>,  
O. Valenzuela<sup>1</sup>, J. Wadsley<sup>5</sup>, T. Quinn<sup>1</sup>

<sup>1</sup>*Department of Astronomy, University of Washington, Box 351580, Seattle, WA 98195, USA*

<sup>2</sup>*INAF, Osservatorio Astronomico di Brera, via Brera 29, 20121, Milano, Italy*

<sup>3</sup>*NYU, Department of Physics, 4 Washington Place, New York, NY 10003*

<sup>4</sup>*ETH, Ramistrasse 101, CH-8092 Zurich.*

<sup>5</sup>*Department of Physics and Astronomy, McMaster University, Hamilton, Ontario L8S 4M1, Canada*

26 June 2018

## ABSTRACT

We used fully cosmological, high resolution N-body + SPH simulations to follow the formation of disk galaxies with rotational velocities between 135 and 270 km/sec in a  $\Lambda$ CDM universe. The simulations include gas cooling, star formation, the effects of a uniform UV background and a physically motivated description of feedback from supernovae. The host dark matter halos have a spin and last major merger redshift typical of galaxy sized halos as measured in recent large scale N-Body simulations. The simulated galaxies form rotationally supported disks with realistic exponential scale lengths and fall on both the I-band and baryonic Tully Fisher relations. An extended stellar disk forms inside the Milky Way sized halo immediately after the last major merger. The combination of UV background and SN feedback drastically reduces the number of visible satellites orbiting inside a Milky Way sized halo, bringing it in fair agreement with observations. Our simulations predict that the average age of a primary galaxy’s stellar population decreases with mass, because feedback delays star formation in less massive galaxies. Galaxies have stellar masses and current star formation rates as a function of total mass that are in good agreement with observational data. We discuss how both high mass and force resolution and a realistic description of star formation and feedback are important ingredients to match the observed properties of galaxies.

**Key words:** galaxies: evolution — galaxies: formation — methods: N-Body simulations

## 1 INTRODUCTION

In a universe dominated by Cold Dark Matter (CDM) and a cosmological constant (Blumenthal et al. 1984; Bardeen et al. 1986; Spergel et al. 2003; Peebles & Ratra 2003), galaxy formation and evolution is a complex combination of hierarchical clustering, gas dissipation, merging and secular evolution. While gravity drives the bottom-up assembly of cosmic structures (Davis et al. 1985), gas cools at the centers of dark matter halos and acquires angular momentum through tidal torques from nearby structures

(Fall & Efstathiou 1980; Fall 1983). Cool gas eventually fragments due to Jeans instabilities and forms stars (White & Rees 1978; Peebles 1969). Gravitational interactions between galaxies can instigate star formation and transform disks into spheroids (Toomre & Toomre 1972) and may dominate galaxy evolution at early epochs especially in dense environments (Frenk et al. 1985). Secular processes, such as external gas accretion or gas displacement due to bars, may play a more important role in galaxy evolution at later epochs (Valenzuela & Klypin 2003; Debattista et al. 2004; Kormendy & Kennicutt 2004). Galaxy formation in

this framework is a continuous, ongoing process where the observable properties of galaxies are a function of their merging histories, masses and environments (e.g. Shen et al. 2003; Blanton 2003; Brinchmann et al. 2004; Bundy et al. 2005).

N-Body/gasdynamical simulations have become the primary tools with which to model galaxy formation in a cosmological context. They are necessary to follow the evolution of the internal structure of galaxies as well as the complex interplay between baryon cooling and feedback (Lake & Carlberg 1988; Katz 1992; Navarro & White 1994; Barnes & Hernquist 1996; Quinn et al. 1996; Haehnelt et al. 1998; Mac Low & Ferrara 1999; Cen & Ostriker 1999; Thacker & Couchman 2000; Navarro & Steinmetz 2000; Tittley et al. 2001; Sommer-Larsen et al. 2003; Governato et al. 2004). However, numerical simulations have had difficulties reproducing the properties of real galaxies. Early work reported a catastrophic loss of angular momentum in the baryonic component of simulated galaxies, leading to the formation of galaxies dominated by a central concentration of cold baryons (Navarro & White 1994). As predicted by early theoretical models (White & Rees 1978; White & Frenk 1991), simulations without strong energy feedback from stellar processes have also suffered from overly efficient star formation. This causes galaxies to form most of their stellar component as soon as gas is able to collapse and cool within small halos, well before the assembly of the main progenitor (Balogh et al. 2001). Dense clumps of stars and cold gas might then spiral rapidly at the center of the main galaxy due to dynamical friction (Navarro & Steinmetz 1997). These shortcomings resulted in compact galaxies with a central excess of old stars and offset from the observed Tully-Fisher relation (Giovanelli et al. 1997). The offset was  $\sim 1.5$  mag for an  $\Omega_0 = 1$  CDM cosmology (Navarro & Steinmetz 2000; Eke et al. 2001) and  $\sim 0.5$  mag in a high  $\sigma_8$   $\Lambda$ CDM (Eke et al. 2001).

More recently, attention has been drawn to the “missing galaxy problem”. Dark matter only simulations predict over an order of magnitude more subhalos around Milky Way-like galaxies than the number of dwarfs observed around the Milky Way and M31 (Klypin et al. 1999; Moore et al. 1999; Willman et al. 2004). Observations also show that more massive late-type galaxies have older stellar populations than less massive late-type galaxies (MacArthur et al. 2004; Ferreras et al. 2004; Gallazzi et al. 2005), in possible contradiction with the fact that in CDM scenarios less massive halos assemble (on average) first.

The angular momentum and missing galaxy problems have often been linked to two major stumbling blocks for numerical galaxy formation: i) insufficient numerical resolution and ii) inaccurate treatment of feedback due to star formation. Only the most recent

gas dynamical simulations have achieved spatial resolution sufficient to resolve the disk scale lengths of disks. Governato et al. (2004) and Kaufmann & Mayer (2006) have shown that poor mass and spatial resolution might lead to significant numerical angular momentum loss in baryonic disks embedded in dark matter halos. These works suggested that at least  $10^5$  DM particles (and equivalent numbers in gas and star particles) within the virial radius as well as force resolution of  $\leq 1$  kpc are required to faithfully simulate the formation and dynamical evolution of disk systems over cosmic times. Recent simulations (Brook et al. 2004; Abadi et al. 2003; Robertson et al. 2004; Okamoto et al. 2005) that used a large number of particles and a high force resolution have indeed formed galaxies with extended stellar disks. However, most of the galaxies formed in most of these simulations also had a massive spheroidal component or disks only partially supported by rotation.

The impossibility of directly resolving the scales at which star formation and feedback happen (a few pc) makes it necessary to develop simplified models to describe star formation and subsequent energy feedback from supernovae (SNe) at galactic scales (0.1 – 1 kpc) (Efstathiou 2000; Silk 2001; Wada & Norman 2001; Ferrara 2002; Krumholz & McKee 2005; Slyz et al. 2005). In early simulations, thermal energy that was simply added to gas surrounding star forming regions was quickly radiated away, resulting in overcooled gas (Katz 1992). However, heated, diffuse baryons resulting from a proper treatment of feedback may be less susceptible to angular momentum transfer to halo particles (Mo & Miralda-Escude 1996; Eke et al. 2000; Maller & Dekel 2002; D’Onghia 2006). To address this shortcoming, Gerritsen (1997), Yepes et al. (1997) and Thacker & Couchman (2000) modeled the pressure support stimulated by gas turbulence by shutting off cooling on timescales of a few million years, and reported the formation of larger disks. Brook et al. (2004) used a scheme similar to that of Thacker & Couchman (2000) and also found it produced reasonably realistic galaxy disks when applied to simplified cosmological initial conditions. Robertson et al. (2004) used an approach similar to that of Springel (2000) and found that the pressure support produced by their multiphase treatment of the ISM was an important factor in the formation of large disks. Supernova feedback and the UV background, being able to reduce gas retention and accretion in halos with low virial temperature, may also solve the problem of the overabundance of satellites (Quinn et al. 1996; Gnedin 2000; Benson et al. 2002; Dekel & Woo 2003; Monaco 2004; Kravtsov et al. 2004). Other recent papers have investigated the roles of a top heavy IMF (Okamoto et al. 2005) and of massive galaxy outflows driven by QSO activity (Binney et al. 2001; Granato et al. 2004; Di Matteo et al. 2005) in regulating galaxy formation.

In this paper, we study the effect of feedback on the structure and satellites of disk galaxies formed within cosmological halos spanning a significant mass range (from  $10^{12} M_{\odot}$  down to  $10^8$ ). We improve over previous work in two ways. First, the mass and spatial resolution of these simulations are sufficient to resolve (i) the structure of present day disks without being significantly limited by resolution and (ii) the sub-halo population for each galaxy in our sample down to circular velocities of about 20% of their parent halo allowing us study the basic properties of galactic satellites. Second, we use a revised implementation of the star formation algorithm introduced by Katz (1992) combined with the feedback recipe introduced by Gerritsen (1997) and then studied by Thacker & Couchman (2000). Details of our implementation can be found in Stinson et al. (2006) (hereafter S06). In this paper we calibrate the free parameters of our algorithm to accurately describe the star formation in isolated galaxy models of present day galaxies. We then apply this algorithm to cosmological simulations of individual high resolution galaxies spanning a decade in mass and analyze their properties.

We focus our analysis in this paper on three fundamental properties of present day galaxies:

- The abundance and luminosities of galactic satellites.
- The Tully–Fisher and baryonic Tully–Fisher relations (Giovanelli et al. 1997; McGaugh 2005).
- Global star formation histories (SFHs) and  $z = 0$  star formation rates.

In §2, we briefly describe the code and the star formation algorithm. A detailed description of our star formation and feedback algorithm with additional tests to those presented here is presented in S06. In §3, we summarize the cosmological runs performed with a range of feedback algorithms, and in §4–9 we discuss and describe in detail the properties of our simulated galaxies. We plan to explore other aspects of both low and high redshift galaxy formation in future papers.

## 2 THE CODE AND THE STAR FORMATION ALGORITHM

### 2.1 GASOLINE

We used GASOLINE (Wadsley et al. 2004), a smooth particle hydrodynamic (SPH), parallel treecode that is both spatially and temporally adaptive with individual time steps. The version of GASOLINE we used implemented i) Compton and radiative cooling, ii) star formation and a supernova feedback as described in detail in S06 and Katz et al. (1996), and iii) a UV background following an updated version of Haardt & Madau (1996) (Haardt 2005, private communication) starting at  $z = 6$ . The opening angle,  $\theta$ , was 0.55 until  $z = 2$  and 0.75

thereafter, and the time-stepping criterion,  $\eta$ , was 0.2, as in Diemand et al. (2004). The minimum smoothing length allowed is equal to 0.1 times the gravitational softening. Exactly 32 neighbors are used for SPH calculations. An ideal gas of primordial composition is assumed. We calculate the cooling/heating rate and ionization state of each particle by assuming collisional ionization equilibrium and the presence of the time dependent, but uniform UV background. The code treats artificial viscosity as suggested in Balsara (1997). The energy equation is computed asymmetrically (Springel & Hernquist 2002; Evrard 1988; Monaghan 1992). This approach avoids the energy conservation and negative energy problems of the arithmetic and geometric implementations and converges to the high resolution answer as well as other recently proposed methods (Benz 1990; Springel & Hernquist 2002; Wadsley et al. 2004).

### 2.2 The Star Formation and SN Feedback Algorithm

Our star formation (SF) algorithm can be broken down into three main parts: (i) identifying the star forming regions, (ii) forming stars and (iii) treating stellar evolution including such effects as mass loss, SN winds and metal enrichment. The algorithm has only three free parameters:  $c_{\star}$ ,  $\epsilon_{\text{SN}}$ , and  $\beta$ . We define these parameters and summarize the main features of the algorithm below. This algorithm is described in detail in S06.

#### 2.2.1 Criteria for Star Formation

The criteria for a gas particle to become eligible for star formation are: (i) Its temperature is colder than 30,000 K; (ii) Local gas density is higher than  $0.1 \text{ cm}^{-3}$ ; (iii) The gas particle is part of a converging flow measured over the 32 nearest neighbors. We do not require the criterion that gas particles are Jeans unstable (Kawata et al. 2005). A minimum gas overdensity  $\delta\rho/\rho$  is also required to avoid spurious star formation at very high  $z$ . We base the rate at which gas is converted into stars,  $d\rho_{\star}/dt$ , on the relation

$$\frac{d\rho_{\star}}{dt} = \rho_{gas}^{3/2} \quad (1)$$

where  $\rho$  represents the volume density. Using the fact that dynamical time,  $t_{dyn} \propto \rho^{-1/2}$ , we express this as

$$\frac{d\rho_{\star}}{dt} = c_{\star} \frac{\rho_{gas}}{t_{dyn}} \quad (2)$$

where we have introduced a constant efficiency factor  $c_{\star}$  to enable us to calibrate the star formation algorithm to match star formation rates observed for  $z = 0$  galaxies. The mass of star particles formed is fixed to 30% of its parent gas particle initial mass (Okamoto et al. 2005). Once the particle passes the above criteria, to implement Equation (1) in a discrete system we assign

a probability  $p$  that a star will actually be spawned from its parent gas particle:

$$p = \frac{M_{SF}}{M_{GP}} \left(1 - e^{-\frac{c_* \Delta t}{t_{form}}}\right) \quad (3)$$

where we have introduced  $M_{SF}$ , the spawning mass for star particles,  $M_{GP}$ , the mass of the gas particle that is creating the star,  $\Delta t$ , the star formation timescale (one Myr in all of the simulations described in this paper) and  $t_{form}$ , which is either the dynamical time or the cooling time, whichever is longer. Gas particles in dense regions with shorter dynamical times will form stars at a higher probability.

### 2.2.2 Feedback and Metal Enrichment From Supernovae

Our implementation of feedback qualitatively follows the algorithm implemented by Thacker & Couchman (2000). We assume that the energy released into the ISM turns into turbulent motions (at unresolved scales) and is partially dissipated, preventing the gas from cooling and forming stars. We determine the number of Supernova type Ia & II that occur during each time step from Raiteri et al. (1996) using a Miller-Scalo IMF and the stellar lifetimes of stars. We then multiply the number of both SN types that explode by a fraction of the canonical  $10^{51}$  ergs/SN times a fixed efficiency term ( $\epsilon_{SN}$ ), and distribute that energy to the surrounding gas particles. In §2.3.2, we explore efficiency values in the range 0.1 to 0.6. At an efficiency  $\epsilon_{SN} = 0.1$  and with the adopted IMF,  $7.65 \times 10^{47}$  ergs of energy are deposited into the surrounding gas for every one  $M_{\odot}$  of star formed. Energy is distributed using the smoothing kernel over the 32 nearest neighbor particles. In our algorithm the time scale for the cooling shutoff and the amount of mass affected are physically motivated and chosen following typical values from the McKee & Ostriker (1977) and Ostriker & McKee (1988) blast wave model. When energy injection comes from a SNII event we disable the radiative cooling for 30 million years in a number of the nearest neighbor particles that satisfy:

$$\beta M_{SNII} > \frac{4\pi r^3}{3} \rho_{ave} \quad (4)$$

where  $M_{SNII}$  is the mass of supernovae produced in a star in a given timestep,  $r$  is the distance from the star to the gas particle in question and  $\rho_{ave}$  is the local gas density and  $\beta$  is a normalization factor. In §2.3.2, we explore  $\beta$  values in the range 0.05 to 0.2. For each SF event the maximum number of particles that can have the cooling disabled as from eq.(4) is the number of SPH neighbors (32 in our simulations).

Once formed, we treat each star particle as a single stellar population with uniform metallicity. The code also keeps track of mass loss from stellar winds. With the adopted IMF, star particles lose up to 30-40% of

their original mass as their underlying stellar population ages. This mass gets distributed to nearby gas particles. Metals come from both SNe Ia & II. Metal enrichment follows Raiteri et al. (1996). Like energy, metals are distributed using the smoothing kernel over the 32 nearest neighbor particles. We plan to study the metallicity of the baryonic component of our simulated galaxies and to introduce metal lines cooling in future papers.

### 2.3 Using Isolated Galaxy Models to Calibrate the SF and SN Feedback Algorithms

We performed a number of simulations of isolated in equilibrium galaxy models to study the effect of different combinations of the three free star formation parameters ( $c_*$ ,  $\beta$  and  $\epsilon_{SN}$ ) on the properties of galaxies with a quiescent star formation and over a range of masses. Parameters were varied within a range of plausible values suggested by observational constraints. The star formation efficiency parameter  $c_*$  was varied over the range [0.01 - 0.4], the mass factor  $\beta$  over [0.05-0.4] and the SN efficiency  $\epsilon_{SN}$  in the range [0.1 - 0.6] (see Table 1). This is a subset of the parameter space explored in S06 where tests were focused on a Milky Way (MW) sized galaxy. However, it is important to extend tests to less massive galaxies. Hence in this work we followed a complementary approach, focusing on the properties of a much smaller galaxy and then verifying that the best parameters so identified would model realistically star formation in a Milky Way sized halo.

#### 2.3.1 The Galaxy Models

To explore the effects of our feedback recipe we applied it to two galaxy models having different peak circular velocities: 220 (MWiso) and 70 km/sec (DWFiso) respectively (where iso stands for “isolated”). Both models were built as equilibrium configurations using the procedure outlined in Springel (2000). Rather than trying to model specific galaxies, we built models consistent with the trend for smaller galaxies to have smaller bulge components and a larger cold gas fraction in the disk (McGaugh 2005; West et al. 2005). The models include a rotationally supported stellar and gaseous disk, a bulge for the MW model only and a dark matter halo component extending to the virial radius. Stars start with a Toomre parameter  $Q=2$ . Disks are built to be stable to bar instabilities.

The dwarf galaxy has no bulge component and gas contributes 50% to its total disk mass.  $10^5$  particles are in its dark matter halo, and  $1.5 \times 10^4$  gas and  $2 \times 10^4$  star particles are in its disk. The softening length is set to about 0.2 times the disk scale length ( $R_d \sim 1$  kpc). Gas and stars have the same exponential radial distribution. Due to its relatively shallow potential, we

Run	$c\star$	$\beta$	$\epsilon\text{SN}$	SFR $M_{\odot}/\text{yr}$	$\sigma_{gas}$ km/sec	$\sigma_{star}$ km/sec	$R_z/R_d$	Hot/Cold Gas volume ratio
DWFiso01	0.05	0.05	0.1	0.20	12	12	0.23	0.5
DWFiso02 <sup>a</sup>	0.05	0.05	0.2	0.16	14	14	0.31	0.6
DWFiso03 <sup>a</sup>	0.05	0.05	0.4	0.12	17	16	0.22	0.6
DWFiso04 <sup>a</sup>	0.05	0.05	0.6	0.06	35	22	0.27	0.9
DWFiso05	0.20	0.05	0.2	0.18	22	20	0.43	1.0
DWFiso06	0.20	0.10	0.2	0.15	20	16	0.61	1.5
DWFiso07	0.20	0.20	0.2	0.13	18	20	0.5	2.0
DWFiso08	0.20	0.20	0.6	0.03	36	28	0.84	1.6

**Table 1.** Summary of the properties of some of the isolated dwarf runs for a given set of  $c\star$ ,  $\beta$  and  $\epsilon\text{SN}$  parameters. SFR is measured over the whole disk after it has set to a quasi steady rate.  $\sigma_{gas}$  and  $\sigma_{star}$  (the azimuthal velocity dispersions) and  $R_z/R_d$  are measured at two stellar disk scale lengths. The volume ratio between the hot gas ( $T > 10^5$  K) vs colder gas included all gas particles within 2 kpc from the disk plane. <sup>a</sup> Parameters used for the Cosmological Runs

expect this galaxy to be fairly sensitive to the details of the feedback and star formation algorithm.

Our Milky Way model (M<sub>W</sub>iso, the same as in S06) has the structural parameters outlined in Klypin et al. (2002), so providing an excellent fit to the existing data of the matter distribution in our own Galaxy. Our Milky Way disk is modeled by  $4.5 \times 10^4$  star particles and  $10^4$  gas particles with a softening of 325 pc. This resolution is similar to that of our cosmological runs. The stellar bulge to disk ratio is 1:7, and gas contributes about 10% of the total mass in the disk component. Disk scale lengths are 3.5 and 7 kpc respectively for stars and gas (Broeils & Rhee 1997).

### 2.3.2 Comparison Between Models and Observations

A set of 25 runs allowed us to study in more detail the effect of the three free parameters ( $c\star$ ,  $\beta$  and  $\epsilon\text{SN}$ ) in our star formation algorithm on the properties of the DW-Fiso model. In this sub-section, we highlight the main trends of simulated galaxy properties with each of the three parameters to motivate our best choice parameters.

Table 1 summarizes the results of 8 representative DWFiso runs. The parameters used in these 8 runs all produce galaxies with star formation rates (SFRs) that range between 0.03 and 0.20  $M_{\odot}/\text{yr}$  and have velocity dispersions of their cold ( $T < 30,000$  K) gas component that range between 12 and 36 km/sec. These values are all consistent with those observed for nearby dwarf galaxies, aside from the 2 galaxies ( $\epsilon\text{SN} = 0.6$ ) with the largest  $\sigma_{gas}$ . The SFR measured from the SDSS (Brinchmann et al. 2004) for small galaxies with stellar masses around  $10^9 M_{\odot}$  ranges typically between 0.02–0.5  $M_{\odot}/\text{yr}$  and has a median value of 0.2–0.3  $M_{\odot}/\text{yr}$  (Brinchmann et al. 2004). Observed values for the velocity dispersion of the cold gas component in disks range in the 10–30 km/sec range (Pizzella et al. 2004).

Although all of the representative runs produce rea-

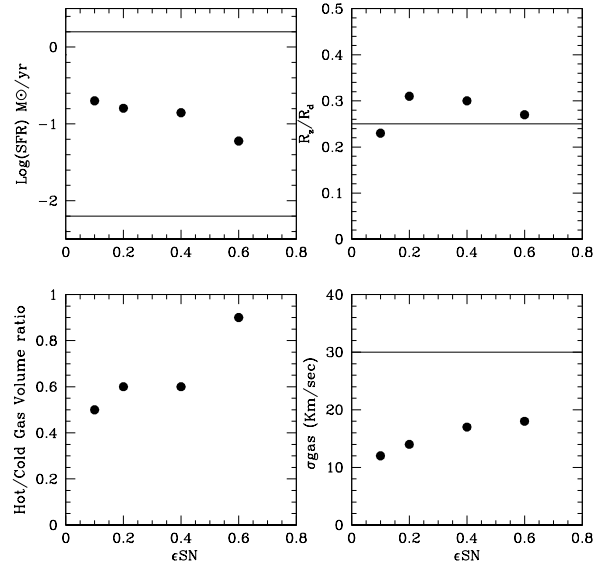


**Figure 1.** Properties of the dwarf galaxy model as a function of  $\epsilon\text{SN}$ . The efficiency parameter  $c\star$  and the mass factor  $\beta$  have both been set to 0.05. Upper left: Star formation rates. The two horizontal lines shows the 95% contour for galaxies of stellar mass  $10^{10} M_{\odot}$  from the SDSS (Brinchmann et al. 2004). Upper right: Disk scale length  $R_d$  vs. the disk scale height  $R_z$ . The horizontal line is the typical value from Bizyaev & Mitronova (2002) and Yoachim & Dalcanton (2006). Lower Left: The hot/cold gas volume ratio as a function of  $\epsilon\text{SN}$ . Lower right: Cold gas velocity dispersion. The horizontal value is the upper value of  $\sigma_{gas}$  from Pizzella et al. (2004).

sonable SFRs and  $\sigma_{gas}$ , only runs with low  $c\star$  (0.05 in the representative sample) produce disks that are thin enough to match observations. The observed ratio of the stellar disk scale height ( $R_z$ ) to stellar disk scale

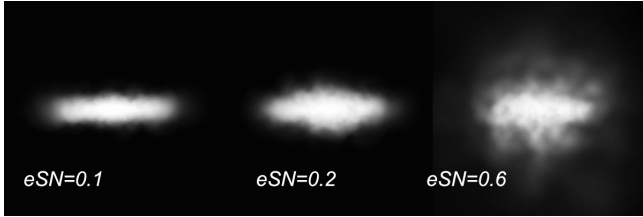


**Figure 2.** The gas projected density for the dwarf galaxy model seen edge on as  $\epsilon\text{SN}$  is varied. The box is 20kpc across.

length ( $R_d$ ) is usually in the range 0.25 - 0.33 for normal disk galaxies (Bizyaev & Mitronova 2002). We find that values of  $c\star$  larger than 0.05 tend to form “thick” disks with a  $R_z/R_d$  ratio larger than observed, possibly because more stars are allowed to form in regions further away from the disk plane. The  $R_z/R_d$  ratio is only weakly dependent on  $\epsilon\text{SN}$  or  $\beta$  (runs 1 through 4, 5, 6 & 7 in Table 1). This suggests that at our resolution low values of  $c\star$  should be preferred to obtain thinner disks. Tests in S06 show  $c\star$  to be weakly dependent on resolution when at least a few tens of thousands gas + star particles are used. However, higher  $c\star$  values have been used when star forming regions are individually resolved (Tasker & Bryan 2005).

As the  $\beta$  factor is increased, more gas is affected by feedback and the volume ratio of the hot/cold phases increases (runs 6,7,8 in Table 1). In our tests we found that runs with the required low values of  $c\star$  tend to form and maintain a large bubble of hot gas in the central region of our models, locally inhibiting star formation, unless  $\beta$  is also low. We thus excluded the region of parameter space with  $\beta > c\star$  from our analysis as being unrealistic.

Figure 2 shows how the gas spatial distribution of the DWFiso model is affected as  $c\star$  and  $\beta$  are fixed to their desired value of 0.05 and  $\epsilon\text{SN}$  is varied from 0.1 to 0.6. In the DWFiso runs, higher  $\epsilon\text{SN}$  leads to lower star formation rates and a higher cold gas turbulence (e.g runs 3, 4, and 8). The SFR of the dwarf galaxy model is most sensitive to the SN energy efficiency parameter  $\epsilon\text{SN}$ , with a realistic SFR obtained with values in the range 0.1-0.6. The images in Figure 2 show that large SN efficiency values create a “galactic fountain” and a patchy gas distribution on the disk plane resembling that of observed small galaxies. However, even with  $\epsilon = 0.6$  only a very small fraction of the gas ejected from the disk plane becomes unbound from the dark matter halo, in agreement with observational evidence and some theoretical expectations (Mac Low & Ferrara 1999; Martin 1999; Mayer & Moore 2004; McGaugh 2005).

Tests on the MWis0 model in S06 preferred values of  $c\star$  in the 0.01–0.1 range but did not constrain  $\epsilon\text{SN}$  significantly due to the relatively deep potential.

For the MWis0 model we set both  $c\star$  and  $\beta$  to 0.05 and varied  $\epsilon\text{SN}$  in the range 0.1 to 0.6 (Table 2). As in S06 the effect of injecting more energy into the ISM is much smaller than for DWFiso, due to the deeper potential well. Increasing  $\epsilon\text{SN}$  by a factor of 6 has a small effect on the properties of the ISM, with  $\sigma_{gas}$ , and the hot/cold gas volume ratio roughly doubling. A smaller “galactic fountain” is created, but only a small fraction of the gas is ejected away from the disk and none actually leaves the boundaries of the surrounding dark matter halo. The vertical velocity dispersion of the stellar disk increases slightly while the SFR decreases by less than 20% across the whole disk. Disk galaxies over a range of stellar masses show a remarkably tight relation between the gas surface density  $\Sigma_{gas}$  and the local surface density of star formation,  $\Sigma_{SFR}$ . Equation 4 of Kennicutt (1998) (originally formulated for the average properties of individual galaxies) states the exact form of this relationship:

$$\Sigma_{SFR} = (2.5 \pm 0.7) \times 10^{-4} \left( \frac{\Sigma_{gas}}{1 M_{\odot} pc^{-2}} \right)^{1.4 \pm 0.15} M_{\odot} yr^{-1} kpc^{-2} (5)$$

As expected from the formulation of eq.5 (Krautsov & Gnedin 2005), star formation across the whole disk of our MWis0 models follows closely the slope of the observed Kennicutt’s law and is shown in Figure 3. Increasing  $\epsilon\text{SN}$  lowers the SFR normalization slightly, again in agreement with the finding from S06.

To summarize the set of tests described in this subsection shows that our SF + SN feedback scheme provides a reasonable match to some of the basic properties of present day, isolated galaxies: Kennicutt’s law, the observed SFR of galaxies, the turbulence of cold gas (at scales of a few kpc) and the thickness ratio of stellar disks. This provides us with some confidence that our simple scheme is able to capture the important aspects of SF and its effects on the ISM of galaxies over a significant range of masses. There is some degree of interplay between the parameters that could be completely captured only by an even larger set of tests. However, it is clear that within the range of parameters explored in S06 and here,  $\epsilon\text{SN}$  predominantly regulates the SFR and the turbulence of the gas.  $\beta$  has to be relatively small to avoid unwanted artificial effects and  $c\star$  plays a relevant role in creating “thin” stellar disks. Given all of the above considerations we have chosen to run our cosmological simulations keeping  $c\star$  and  $\beta$  fixed at 0.05 while varying  $\epsilon\text{SN}$  in the range 0.2 – 0.6.

### 3 COSMOLOGICAL RUNS

For our cosmological runs we selected three galaxy-sized halos (DWF1, MW1 & GAL1) from 28.5 and 100 Mpc boxes, low resolution, dark matter only simulations run in a concordance, flat,  $\Lambda$ -dominated cosmology:  $\Omega_0 = 0.3$ ,  $\Lambda=0.7$ ,  $h = 0.7$ ,  $\sigma_8 = 0.9$ , shape pa-

Run	$c^*$	$\beta$	$\epsilon\text{SN}$	SFR $M_\odot/\text{yr}$	$\sigma_{gas}$ km/sec	$\sigma_{star}$ km/sec	$R_z/R_d$	Hot/Cold Gas Volume Ratio
MWiso1	0.05	0.05	0.1	0.85	12	13	0.04	0.22
MWiso2	0.05	0.05	0.4	0.8	18	20	0.05	0.26
MWiso3	0.05	0.05	0.6	0.7	20	24	0.05	0.4

**Table 2.** Summary of the properties of the isolated Milky Way runs: quantities defined as in Table 1

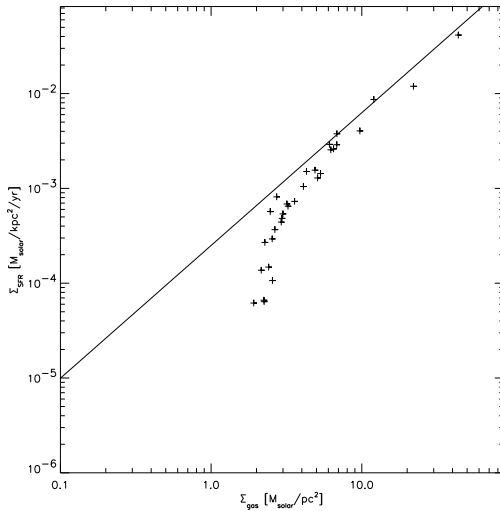


**Figure 3.** Star Formation rate vs local gas surface density. Dots from the MWiso3 galaxy model run ( $\epsilon\text{SN}=0.6$ ). The straight line is a fit to Kennicutt's Law.

parameter  $\Gamma = 0.21$ , and  $\Omega_b = 0.039$  (Perlmutter et al. 1997, Efstathiou et al. 2002). Given the masses and virial radii of the selected halos the sizes of the starting boxes are large enough to provide realistic torques. The power spectra to model the initial linear density field were calculated using the CMBFAST code to generate transfer functions (Zaldarriaga & Seljak 2000). These three halos were resimulated at higher resolution using the volume renormalization technique (Katz & White 1993).

We resimulated DWF1, MW1, and GAL1 to have a similar dynamical range in each simulation. Each galaxy model was resimulated to have a similar number of particles within the virial radius, and the softenings were rescaled so that the spatial resolution of each galaxy was a similar fraction of its virial radius. With our choices of particle number and softening, the smallest subhalos resolved have typical circular velocities of 20% of their host. For all particle species in the high resolution region, the gravitational spline softening,  $\epsilon(z)$ , evolved comovingly from the starting redshift ( $z \sim 100$ ) until  $z=9$ , and remained fixed at their final value from

$z=9$  to the present. The softening values chosen are a good compromise between reducing two body relaxation and ensuring that disk scale lengths and the central part of dark matter halos will be spatially resolved (see Diemand et al. 2004 for a number of relevant tests). Integration parameter values were chosen as suggested in Moore et al. (1998) and then confirmed in Power et al. (2002).

We selected a halo mass range to study halos associated with typical disk galaxies. The three selected halos have masses of  $1.6 \times 10^{11}$  (DWF1),  $1.15 \times 10^{12}$  (MW1), and  $3.1 \times 10^{12} M_\odot$  (GAL1) measured within their virial radius  $R_{vir}$  (the radius enclosing an overdensity of 100 times the critical density  $\rho_{crit}$ ). GAL1, the largest halo, is more massive than that of our Milky Way, as a recent analysis points to a Milky Way halo of about  $10^{12} M_\odot$  (Klypin et al. 2002). This is the mass of our intermediate size halo (MW1). Our least massive halo, DWF1 corresponds to that of a typical disk field galaxy. The three galaxies span a range of circular velocities  $V_c$  (measured at  $R_{vir}$ ) and defined as  $\sqrt{M}(r < R)/R$  between 70 and 185 km/sec. Note that this  $V_c$  is defined differently than the  $V_{rot}$  used later in the paper. Dark matter particle masses in the high resolution regions were  $7.6 \times 10^5$ ,  $6.05 \times 10^6$  and  $2.3 \times 10^7 M_\odot$  and the spline softening was 0.3, 0.6 and 1 kpc for DWF1, MW1 & GAL1 runs, respectively. The MW1 halo was also run at higher resolution to test resolution effects. The results of the resolution testing are in §8. GAL1 is the same halo described in Governato et al. (2004). The main halo properties are summarized in Table 3.

The merging histories and angular momentum of parent dark matter halos play a major role in defining the final properties of the galaxies that form inside them (Cole et al. 2000). It is therefore important to make sure that our halos have merging histories and spin parameters somewhat representative of the global population. The three galaxies were selected with the only criteria of the redshift of their last major merger ( $z_{lmm}$ )  $> 2$  and with no halos of similar or larger mass within a few virial radii. A major merger is defined here as having a 3:1 mass ratio. The three halos have formation times (defined as the main progenitor achieving 50% of its final mass) in the 0.6 – 1.5 redshift range. Their spin parameter,  $\lambda$  (defined as  $JE^{1/2}/GM^{5/2}$ ) varies from 0.01

Run	Virial Mass $M_{\odot}$	Virial Radius kpc	$V_c^a$ km/sec	Formation time z	$\lambda$	Last major merger z	$\epsilon$ kpc	$N_{tot}^b$ at z=0 dark+gas+stars
DWF1	$1.6 \cdot 10^{11}$	142	70	1.5	0.01	2.3	0.3	$\sim 860.000$
MW1	$1.15 \cdot 10^{12}$	271	134	0.6	0.07	2.5	0.6-0.3 <sup>1</sup>	$\sim 700.000 - 4.000.000^1$
GAL1	$3.1 \cdot 10^{12}$	380	185	0.96	0.035	2.75	1.	$\sim 480.000$

**Table 3.** Summary of the properties of the three cosmological halos: <sup>a</sup> Circular velocity at virial radius, <sup>b</sup> number of gas and star particles changes slightly depending on  $\epsilon$ SN. <sup>1</sup> smaller/larger values are for the z=0.5 Super High Res. Run. respectively

for DWF1 to 0.05 for MW1, with the average value for cosmic halos  $\sim 0.035$  (Gardner 2001).

$z_{lmm}$  is likely a crucial parameter in defining the properties of a galaxy disk (Steinmetz & Navarro 2002). If mergers efficiently destroy disks, a low  $z_{lmm}$  would leave less time to grow a new stellar disk from newly accreted gas (Baugh et al. 1996). We therefore stress that the  $z_{lmm}$  of these three halos is close to the average of the population of galaxy sized halos in our adopted cosmology, as measured in a recent large set of N-body simulations (Li et al. 2005). The same authors showed that previous estimates of the average  $z_{lmm}$  estimates based on the extended Press & Schechter approach were biased towards lower z's. DWF1 has its last major merger at z=2.3, when a head-on encounter generates a very prolate halo. It only accretes relatively small halos after that. After its last major merger at z = 2.5, MW1 has a counter rotating minor merger at z = 2. A relatively high  $z_{lmm}$  for the MW1 halo is consistent with the Milky Way forming several Gyrs ago (Wyse 2002). At z = 2.75, GAL1 undergoes multiple mergers and accretes several satellites after that. A few get disrupted after several passages through its disk. In the future, we plan to simulate the formation of galaxies with a wider range of initial conditions.

For each halo a sequence of runs of increasing complexity was performed. Table 4 summarizes these runs. For the MW halo initial conditions, we performed the following runs: DM only (MW1dm), no gas cooling or SF (MW1ad), no feedback and no UV (MW1g0), UV turned on but without stellar feedback (MW1g1), and three runs with various supernova efficiencies (MW1g2 to MW1g4). In all runs with SF we kept the star formation efficiency fixed and the mass factor  $\beta$  and varied only the fraction of energy from SN dumped into the ISM  $\epsilon$ SN from 0.2 to 0.6. Based on the results from §2 we will mainly focus on the properties of the runs with a SN energy efficiency of 40% ( $\epsilon$ SN=0.4). Results from the cosmological runs confirm a posteriori this choice: a higher SN efficiency creates a DWF1 galaxy with an unrealistic low cold gas mass fraction in the disk ( $< 3\%$ ).

Our MW1g4 ( $\epsilon$ SN=0.6) run of the MW1 halo was repeated at eight times better mass resolution and 2 times better spatial resolution (run MW1hr in Table 4). The run was stopped at z=0.5 due to its computational

run	c*	$\beta$	UV	$\epsilon$ SN
DWF1g1	0.05	-	off	off
DWF1g2	0.05	0.05	on	0.4
DWF1g3	0.05	0.05	on	0.6
MW1dm	dm only			
MW1ad	no SF, no cooling			
MW1g0	0.05	-	off	off
MW1g1	0.05	0.05	on	off
MW1g2	0.05	0.05	on	0.2
MW1g3	0.05	0.05	on	0.4
MW1g4	0.05	0.05	on	0.6
MW1hr	0.05	0.05	on	0.6
GAL1g1	0.05	0.05	on	off
GAL1g2	0.05	0.05	on	0.2
GAL1g3	0.05	0.05	on	0.4

**Table 4.** Main Parameters of Cosmological Galaxy Runs

cost. With four million resolution elements within the virial radius, a star particle mass of  $3 \times 10^4 M_{\odot}$  and a force resolution of 0.3 kpc, this run has likely the highest resolution ever achieved for a Milky Way sized galaxy simulation carried to a relatively small redshift. We will use this simulation to test the effects of increasing resolution in §8.

#### 4 THE EFFECT OF FEEDBACK ON THE PROPERTIES OF SATELLITES

To explore the effect of UV and supernova feedback on satellites, we compare the properties of satellites within the virial radius in the six MW1 simulations described in Table 4. The MW1 satellites are the most easily comparable to the satellites of our own Milky Way (Mateo 1998). Unless specified, similar qualitative conclusions apply to DWF1 and GAL1. We will present a much more detailed analysis of the satellites in a subsequent paper. Subhalos were identified using SKID (Governato et al. 1997) and only those with at least 64 DM particles were used in the analysis. That minimum number of dark matter particles translates to minimum dark matter masses of: 0.49, 3.9, and  $14.9 \times 10^8 M_{\odot}$  so-



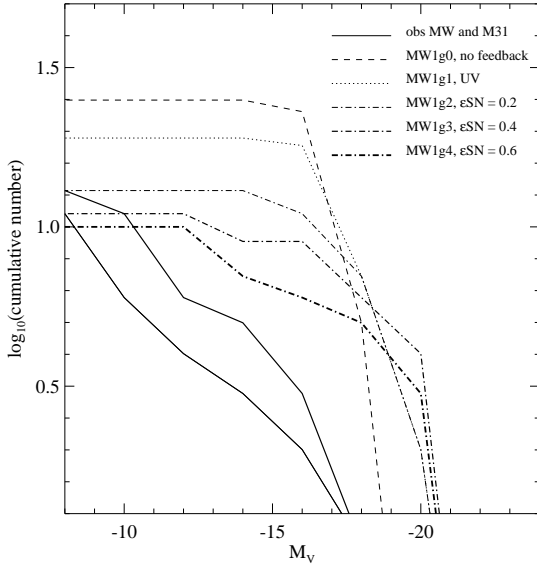


**Figure 4.** The luminosity functions of satellites within  $R_{vir}$  in all 4 MW1 runs, compared with the luminosity functions of both the Milky Way’s and of M31’s satellites. Only satellites containing at least 64 DM particles are included. The 2 runs without supernova feedback produce far too many satellites. However, all 3 of the runs including supernova feedback produce a number of satellites that reasonably matches that of the Milky Way and M31 satellite populations (lower and upper solid lines respectively), although the simulated satellites are still too bright.

lar masses for the satellites of DWF1, MW1, and GAL1 respectively. The resolution limit translates into a circular velocity limit of  $V_c \sim 20\text{--}30$  km/sec depending on the individual satellite density profile. We use the ages and metallicities of each star particle in the satellites to determine their absolute V-band magnitudes assuming no dust reddening. Satellites have a mean (not luminosity weighted) B-V of 0.63. We verified that field dwarfs have slightly bluer colors.

Figure 4 shows the satellite luminosity functions of the MW1 cosmological runs compared with those observed for the Milky Way and M31. A comparison of both the g0 and g1 simulations (no feedback; then UV on, but no SN feedback) with the observed satellite luminosity functions of the Milky Way and M31 highlights the missing satellite problem. On the contrary, runs including SN feedback result in satellite populations similar in number, although not in luminosity, to the observed populations. The total number of luminous satellites is not strongly dependent on the strength of feedback implemented in the S06 algorithm.

Although both g0 and g1 have a total of 26 satel-

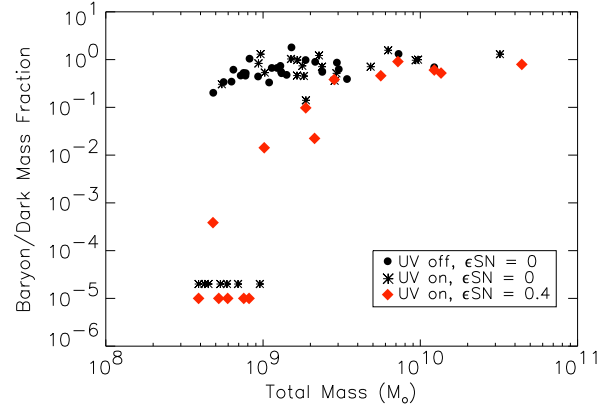


**Figure 5.** The baryon to DM ratio for all the subhalos within  $R_{vir}$  of the MW1 galaxy. With no UV field or SN feedback the baryon fraction is constant down to our resolution limit of 64 DM particles. UV creates some dark satellites, while SN feedback removes a substantial fraction of baryons from halos with total masses below a few times  $10^9 M_\odot$ . Note that total satellites masses have been affected by tidal stripping. Halos with no baryons in the UV only run have been shifted upward for clarity.

lites, the runs including supernova feedback all have 20 or fewer satellites total, only some of which host stars. This difference in total satellite number occurs because simulations with more severe overcooling form satellites very centrally concentrated and less susceptible to tidal effects and complete disruption (see also Macciò et al. 2005). Similarly, runs with cooling but no SN feedback (as MW1g0 and MW1g1) contain  $\sim 2x$  the number of satellites as the DM only run or the run with no gas cooling.

Figure 5 shows that some of the satellites in the runs including UV are completely devoid of stars. There are no satellites within  $R_{vir}$  in any of the simulations that retain gas but don’t contain any stars. Unlike UV feedback, supernova feedback can also expel gas from the satellites once they start forming stars, reducing the overall baryon fraction of satellites containing stars. These reduced baryon fraction satellites are seen in Figure 5. As expected, the satellites of the run with stronger supernova feedback have a smaller baryon fraction than the run with weaker supernova feedback. The luminosity functions of satellites in the MW1 (and of GAL1) simulations show that the introduction of SN feedback in particular is essential to reproduce the observed number of satellites in Milky Way type galaxies. The number of satellites containing stars appear is fairly robust as resolution is increased (see Fig.20). At a higher resolution while tens of less massive dark satellites are resolved, only a few more are able to make stars. This is

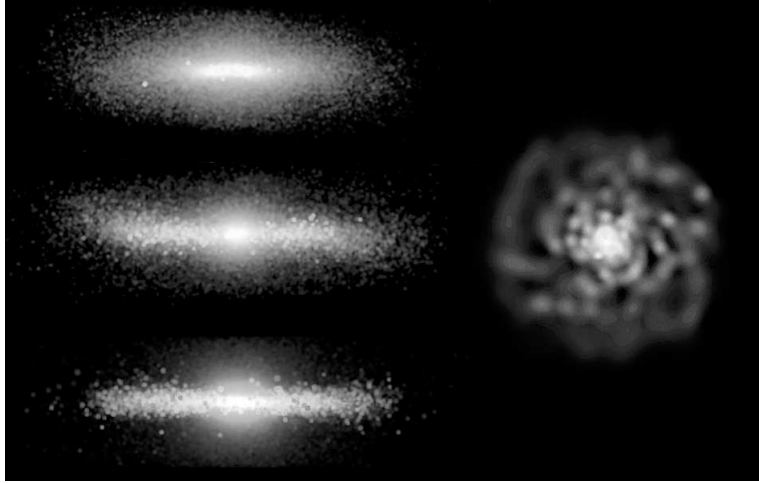


**Figure 6.** Left panel: Brightness maps of the edge-on disks of (from top to bottom) GAL1, MW1 and DWF1 at  $z=0$ . Each star particle in the simulations has been weighted by its age-dependent bolometric luminosity. Right Panel: the face-on surface density of the gas for DWF1 at  $z=0$ . Each frame is 30 kpc across

because the mass threshold below which the UV field makes satellites completely dark (Quinn et al. 1996) is resolved in our runs (Fig.5). All but one satellite of galaxy DWF1 (the run with the best mass resolution in our set) are completely dark when SN feedback is on. Note that the list of known MW satellites at very low luminosities and surface brightnesses might still be incomplete (see Willman et al. (2004) for a discussion).

## 5 PROPERTIES OF THE DISKS

The images in Figure 6 show that all three galaxies have formed a significant stellar disk by redshift  $z=0$ . In this section, we discuss in detail the spatial and kinematic properties of the disks, investigate the effects of feedback on disk properties, and demonstrate the formation of the disks during major, gas-rich mergers.

### 5.1 Density Profiles of the Disks

The top panel of Figure 7 shows the  $z=0$  stellar surface density profiles of the disks as a function of radius for our fiducial runs (DWF1g2, MW1g3, GAL1g2 -  $\epsilon$ SN=0.4). Hereafter we will simply refer to these specific runs as DWF1, MW1, and GAL1 as we report and discuss our results. We include all stars within 4 disk scale heights,  $R_z$ . The stellar disk component of all galaxies is well-fit by an exponential distribution between one and three disk scale lengths. The profiles in Figure 7 illustrate that all galaxies also show evidence for a central, steeper component that extends to 1 or 2 kpc.

Disk scale lengths,  $R_D$ , were measured by fitting an exponential profile to the disk component, but excluding the steep central component and stopping where the surface density shows a break. To approximate the effect of measuring the disk scale length in different optical

bands, we measured the scale lengths of stars in different age ranges:  $< 2$  Gyrs,  $< 4$  Gyrs and  $< 11$  Gyrs, to approximate the B, R and K optical bands, respectively (Martin et al. 2005). These scale lengths are summarized in Table 5. The bottom panel of Figure 7 shows the stellar density profiles of MW1 in each of these three stellar age ranges. Beyond 2.5–3 scale lengths (shown by the outer vertical line), the disk surface density declines rapidly for the youngest stars. These disk profiles are quite common in observed spiral galaxies (Pohlen & Trujillo 2005; Florido et al. 2001). In the remainder of this section we will refer mostly to stars younger than 4 Gyr (R band) to illustrate our results, unless otherwise specified.

The exponential disk component forms from the inside out as observed in many disk galaxies (Ryder & Dopita 1994). However, gas inflow due to the late formation of a bar or an oval-like structure in the central few kpc, which is responsible for the observed central steepening of the profile, can trigger enhanced star formation in the inner disk, which then forms partially outside-in. This mode of disk formation is significant in run GAL1 and was already reported in Governato et al. (2004). At  $z=0$ , star formation in GAL1 is primarily concentrated in the inner parts of the disk. The scale length of stars younger than 2 Gyr in GAL1 is only 1.1 kpc, half that of the older component. This is typical of massive S0/early type disk galaxies (Pohlen et al. 2004).

All three galaxies have extended disks of gas colder than a few  $10^4$  K with exponential scale lengths larger than even the youngest stellar disk component, as in Ryder & Dopita (1994). The right panel of Figure 6 shows that at our sub-kpc resolution and with our feedback scheme we are able to qualitatively capture the

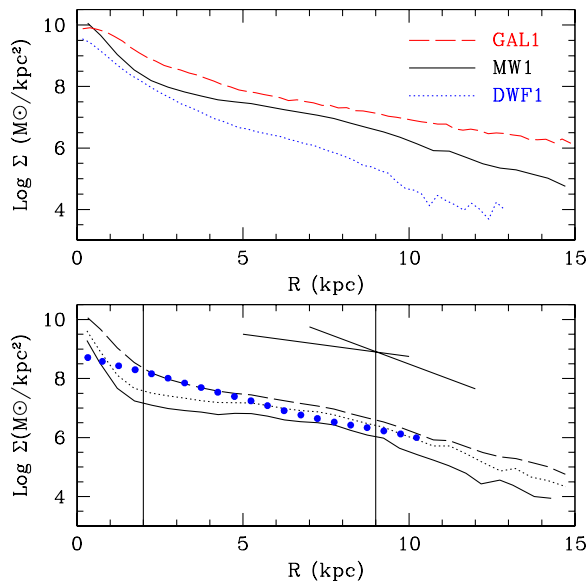


**Figure 7.** The face-on stellar density profile of the three simulated galaxies. Only stars within  $4 R_z$  from the disk plane are considered. The upper panel shows the contribution from all stars with a cosmic age between 0 and 10 Gyrs, roughly corresponding to the K band (Martin et al. 2005). The lower panel shows the projected stellar density profile of the MW1 galaxy for stars in the 0–3 Gyrs (solid), 0–4 Gyrs (dotted) and 0–10 Gyrs (dashed) age range. Dots show the stellar profile of the MW1hr at  $z = 1.7$ . The two straight lines show the slope of the younger stellar component inside and outside the break radius.

complex nature of the ISM. The gas distribution in the disk plane of our smallest galaxy (DWF1) and in the high resolution MW (MW1hr) shows a complex structure of spiral arms linked by filaments and surrounded by a hotter medium.

The stellar profile of the final disks in the more massive galaxies (MW1 and GAL1) is only weakly dependent on the strength of supernovae feedback as we allow the energy efficiency to vary only by a factor of three, being constrained by the early tests we carried in §2. Okamoto et al. (2005) showed how the density distribution might depend substantially on the feedback adopted. It is likely that the energy injection per unit mass in the feedback scheme adopted by Okamoto et al. is higher than in our simulations. Instead, the disk stellar profile of DWF1, our less massive galaxy, is more affected when varying the amount of SN feedback in the same range (Fig.8). When  $\epsilon$  increases to 0.6 the stellar density profile of younger stars in DWF1 is best described by a single, exponential profile with a shorter scale length and truncated at about  $2 R_d$ . Similarly to the tests performed in §2 the cold gas is much more

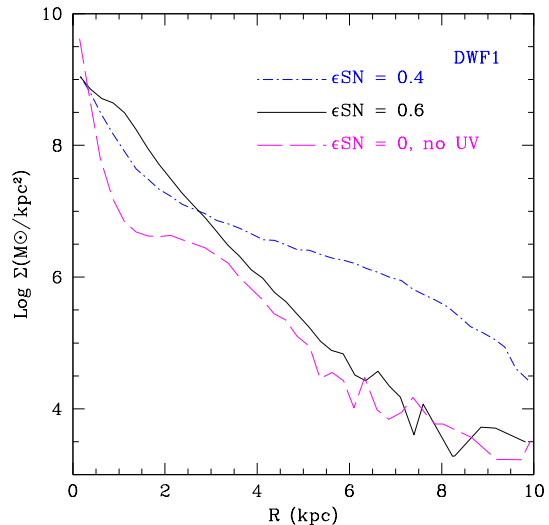


**Figure 8.** The face-on stellar density profile of the DWF1 galaxy as a function of feedback strength. Only stars within  $4 R_z$  from the disk plane and in the 0–4 Gyrs age range are plotted.

turbulent, making star formation inefficient at low densities. When feedback is turned off cold gas settles in a smaller, more compact disk that originates a denser central core. As the disk surface density increases the disk becomes bar unstable redistributing the stellar material and originating the “flat” stellar profile at  $\sim 2\text{kpc}$  that is usually associated with strong dynamical instabilities (Debattista et al. 2005). In all three galaxies runs without feedback form “hotter” stellar disks with a higher scale length.

## 5.2 Kinematics of the disks

We first studied the dynamical properties of the simulated objects and verified that the disks are indeed supported by rotation. For every star particle within the “disk” we computed  $J_z$ , the component of angular momentum parallel to the total angular momentum of all disk stars. We defined the disk stars as those within  $4 (R \text{ band})$  scale lengths and heights centered on each galaxy. We compared  $J$  along the  $z$  axis to the angular momentum of the co-rotating circular orbit with similar orbital energy,  $J_c(E)$ . Stars in a disk compo-

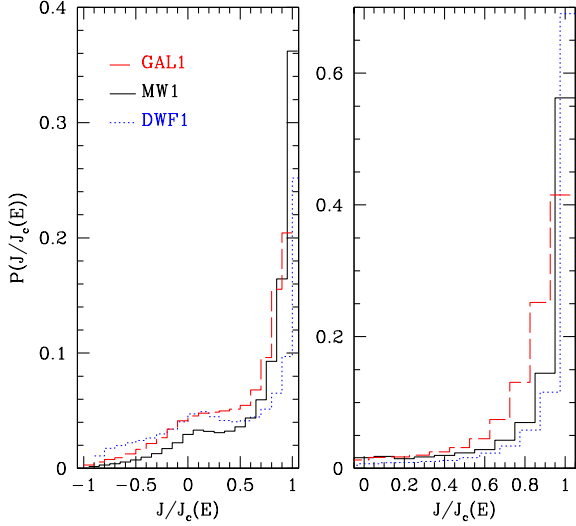


**Figure 9.** Mass weighted probability distributions of the orbital circularity  $J/J_c$  for disk stars in DWF1 (solid), MW1 (dotted) and GAL1 (dashed). The right panel (note the change of scale) shows only star particles formed in the last 3 Gyrs.

ment completely supported by circular motions should by definition have  $J/J_c = 1$ . Figure 9 shows the mass weighted distribution for all the disk star particles (left panel) and for disk star particles formed in the last 3 Gyrs (right panel). The histogram distributions show clearly that in all three galaxies the disk component is mostly supported by rotation. Our DWF1 and MW1 galaxy models have a higher fraction of stars on circular orbits when compared with the distributions showed by Abadi et al. (2003) and Okamoto et al. (2005). In particular the young stellar component is heavily dominated by stars on almost circular orbits: 80% of young stars in the DWF1 run have  $J/J_c > 0.8$ . 62% of all stars in the MW1 galaxy have  $J/J_c > 0.8$ . As a comparison most thin disk stars in the MW have  $J/J_c > 0.7$  (Nordström et al. 2004). A central hump in the  $J/J_c$  distribution, that has often been interpreted as the sign of a massive halo/bulge component is evident in the DWF1 run. We verified that the low angular momentum stars are also the oldest, and were formed during DWF1’s last major merger.

The amount of stellar rotation versus velocity dispersion,  $v/\sigma$ , is another good measure of how realistic are the disks that we obtained:  $V_{rot}/\sigma \sim 4$  for the MW1 disk stars younger than 4 Gyrs, where  $\sigma$  is the rms average between the tangential and radial velocity dispersions. Typical observed values range from 2 to 5

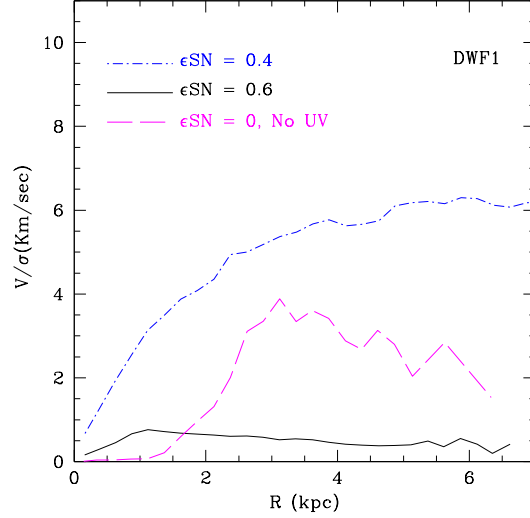


**Figure 10.** The  $V/\sigma$  ratio for the young stellar component of DWF1 as feedback is increased: Long dashed: no feedback or UV, dot dashed:  $\epsilon\text{SN} = 0.4$ , solid:  $\epsilon\text{SN} = 0.6$

for the disks of normal galaxies (Pizzella et al. 2004). Fig.10 shows  $V_{rot}/\sigma$  for the young stellar component of DWF1. The dynamically coldest stellar disk is obtained with  $\epsilon\text{SN} = 0.4$ . Stronger feedback makes the ISM more turbulent, causing stars to form with a higher velocity dispersion. For all three galaxies runs without SN feedback generate stellar disks with lower  $V_{rot}/\sigma$  ratios, due to stronger loss of angular momentum driven by bar instabilities or because the velocity dispersion is increased by the overall stronger heating by satellites (that survive disruption much closer to the galaxy center). These statements hold true irrespective of the selected age interval for the stars.

The azimuthally averaged rotation curves of galaxies are shown in Figure 11. Both the rotation curve of the cold gas component and of the disk stars younger than 4 Gyrs are plotted. For both the MW1 and DWF1 runs intermediate age stars and cold gas have very similar profiles, confirming that younger stars are in orbits close to circular. In the GAL1 run (our most massive galaxy), the stellar and gaseous disks are not completely coplanar. This offset creates a difference in the central part of the velocity profile of the two components. The outer part of GAL1’s stellar disk is also dynamically

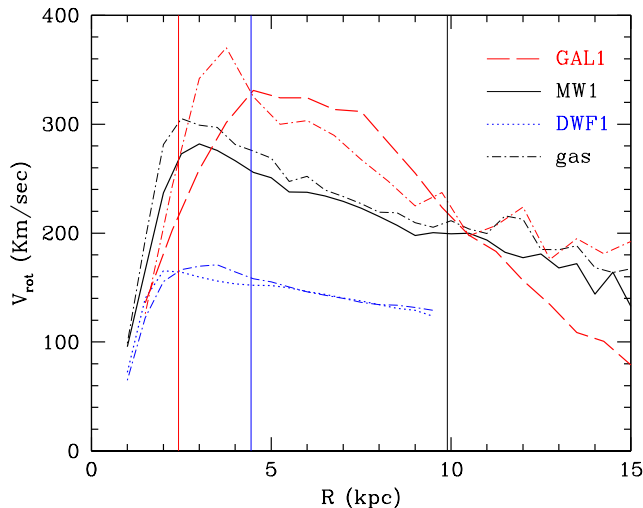


**Figure 11.** Azimuthally averaged rotation velocity of cold gas (dot – dashed line) and stars (age < 4 Gyrs). From top to bottom: GAL1, MW1, DWF1. The vertical lines show  $2.2 R_d$  for each galaxy.

hot, which makes  $V_{rot}$  of the stellar component decline very rapidly at outer radii.

While all our galaxies show long lasting bar instabilities, the introduction of SN feedback increases the stability of the disk and thus reduces the non-axisymmetry of the stellar disk. Stronger feedback generates stronger disk axisymmetry. In all simulations with feedback, only an oval distortion with scale smaller than the disk scale length is present as opposed to a clear bar with scale length  $\sim$  disk scale length in models without SN feedback. The small oval distortion is likely an unresolved bar, because our high resolution control run (MW1hr) does display a resolved bar at its center. Disks with feedback are more stable to bar formation because their stellar disk builds up more slowly over time.

We can understand the stabilizing effect of feedback by comparing the mass in the halo to that in the disk using the parameter  $\varepsilon = (V_{max} \times R_D) / GM_d$ , introduced by Efstathiou et al. (1982) to measure the susceptibility of disks to bar formation.  $V_{max}$  is the peak circular velocity and  $M_d$  and  $R_D$  are, respectively, the mass and exponential scale length of the disk. Numerical experiments (Efstathiou et al. 1982; Mayer & Wadsley 2004) show that  $\varepsilon > \alpha$ , with  $0.95 < \alpha < 1.1$ , is required for stability against bar formation of a disk of gas and stars (the higher the gas fraction, the higher  $\alpha$ ). Measuring  $\varepsilon$

in a cylinder within 0.5 kpc of the disk plane, we find that in the runs without feedback  $\varepsilon$  is already  $< 0.9$  at  $z > 1$ . In the runs with feedback,  $\varepsilon$  does not approach unity until near  $z = 0$ . In runs without feedback the disk is more massive and denser at earlier epochs, and thus more bar-unstable. Without feedback, all the gas that is accreted rapidly makes disk stars, while with feedback a significant fraction of the baryons remain hot and diffuse and do not form stars even when they reach the disk. A visual comparison with real rotation curves shows that our simulated galaxies produce rotation curves that raise rapidly and then decline too fast at  $R > 4 R_d$ . Only DWF1 has a rotation curve close to being “flat” as observed for most normal spiral galaxies (Catinella et al. 2006). This is likely due to a combination of a still too massive central component and the outer part of disks being affected by two body heating from halo particles.

### 5.3 Gas Rich Mergers and the Formation of Disks at High Redshift

With our relatively high resolution we are able to follow the formation of disks early on in our simulations. Perhaps surprisingly, the disk of the MW1 galaxy starts forming immediately after the last major merger event confirming early results by (Springel & Hernquist 2005) and (Elmegreen et al. 2005) that gas rich mergers with substantial feedback are conducive to the observed early formation of disks (Trujillo et al. 2005). In our simulations feedback stops a substantial fraction of gas from turning into stars during the major merger. 40% of the mass of the disk of MW1 is gas at  $z = 2$ . With lots of orbital angular momentum available from the merger, gas cools and rapidly settles into an extended exponential disk, especially in runs with stronger feedback and higher resolution. Even for DWF1 and GAL1, substantial stellar disks form immediately after  $z_{tmm}$ . Without feedback a much more compact stellar component forms and becomes rapidly non-axisymmetric, as described in §5.2. At  $z > 1$  stellar disks are 20-30% larger when feedback is on, although by  $z = 0$  their sizes are virtually identical.  $V/\sigma$  measured in the disk of the high resolution MW1hr run is  $\sim 1.6$  at  $z = 1.5$  for stars that form shortly after  $z_{tmm}$ . This stellar component is heated by a combination of the rapidly changing central potential and by a couple of minor satellite accretions onto the disk that occur before  $z = 1.5$ . This early disk could be associated with the thick disk components of present day spiral galaxies (Seth et al. 2005; Yoachim & Dalcanton 2005; Brook et al. 2004).

### 5.4 Bulge & Disk Decomposition

To separate the bulge, disk and halo components we assigned to the “bulge” all stars in the age range that

Run	Rd <sub>B</sub>	Rd <sub>R</sub>	Rd <sub>K</sub>	Rz <sub>R</sub>	Rd <sub>gas</sub>	Rz <sub>gas</sub>	B <sub>Tot</sub>	I <sub>tot</sub>	K <sub>Tot</sub>	SFR <sup>1</sup> M <sub>⊙</sub> /yr	V <sub>c</sub> <sup>2</sup>	M <sub>★</sub>
DWF1	2.02	1.95	1.2	0.3	7.	0.4	-19.8	-21.2	-22.6	0.6	160	1.38 × 10 <sup>10</sup>
MW1	4.5	3.8	2.1	1.	10	1.	-21.1	-22.6	-24	2.2	205	4.6 × 10 <sup>10</sup>
GAL1	1.1	1.2	2.15	2.3	6.	1.3	-22.0	-23.5	-24.9	7.1	180	1.36 × 10 <sup>11</sup>

**Table 5.** Summary of the properties of the disks of the galaxies formed in the cosmological runs (only runs with  $\epsilon\text{SN} = 0.4$  are shown). <sup>1</sup> at  $z=0$ , <sup>2</sup> at  $2.2 R_d$ .

would give a  $V_{rot}/\sigma < 1$  and within four disk vertical scale heights from the disk plane. This selects an old, slowly rotating stellar component. Disk stars were those within four disk scale heights and scale lengths that were not assigned to the bulge. Stars not belonging to the bulge, disk or individual satellites were assigned to the halo. The kinematically defined B/D mass ratio of the fiducial MW1 is  $= 0.3$  or smaller. This result does not change for other reasonable decomposition techniques (Governato et al. 2004). We only used dynamical definitions of the galaxy components. A photometric decomposition was not attempted but given that stars in the disks are younger and then brighter it is likely that a luminosity weighted estimate would give a lower B/D ratio. We speculate that the low B/D ratio of the MW1 is due to the high angular momentum acquired by cold gas during the last major merger event. The DWF1 and GAL1 simulations both formed a more massive “bulge”. This result is likely a consequence of different physical processes: (i) The DWF1 galaxy has very low angular momentum (the last major merger at  $z = 2.3$  is almost head-on); (ii) GAL1 forms stars in its central region until the present time, as gas keeps cooling from the surrounding halo. Its bulge has fairly blue colors and is relatively more massive. The relevant scale lengths are  $< 1$  kpc, so we decided to postpone a more detailed analysis of the bulge components of our simulated galaxies when higher resolution simulations will be available.

## 6 MATCHING THE TULLY – FISHER RELATION

The Tully–Fisher (TF) relation links the characteristic rotation velocity of a galaxy with its total absolute magnitude (Giovanelli et al. 1997). Similarly, the “baryonic TF” relation (McGaugh et al. 2000; McGaugh 2005) links characteristic rotation velocity with total disk mass to account for the fact that less massive galaxies are more gas rich and thus that their stars only account for a small fraction of their disk total mass. Both relations imply that the total disk mass and its radial distribution are closely connected with the total mass of a halo. Early simulations matched the slope of the TF relation, but reported (Eke et al. 2001) difficulties in matching its normalization. The relatively weak feedback adopted in that work might have caused

galaxies to cease star formation relatively early, leaving the disks too red and then causing the TF relation offset. Alternatively, the central rotational velocities of the simulated galaxies were too high due to an excess of matter at the center of galaxies possibly due to excessive baryonic cooling and the subsequent adiabatic contraction of the dark matter component. Even high resolution simulations like Governato et al. (2004) and Abadi et al. (2003) have shown a consistent offset from the TF relation of late type spirals, with galaxies being too centrally concentrated compared to real ones. Compared to some previous works our simulations have sufficient resolution to allow us a much direct comparison with observational data as  $V_{rot}$  is now measured at only a few kpc from the center. This poses a much stronger constraint on simulations as they have to reproduce the stellar mass distribution and kinematics at relatively small scales.

When feedback is included, simulations successfully match both the TF and baryonic TF relations, this result being possibly the most important conclusion of the work presented here: it shows that our simulations produce a realistic distribution of stars, baryons and DM within the central few kpc. To compare our simulations with the observed TF relations, we used the rotation curves plotted in Figure 9 (and described in §5.2) to determine  $V_{rot}$  measured at 3.5 disk scale lengths for DWF1, MW1, and GAL1 as in the Giovanelli sample. We then obtained the global magnitudes for each galaxy model by coupling the star formation histories (SFHs) of our simulations with GRASIL (Silva et al. 1998), a code to compute the spectral evolution of stellar systems taking into account dust reprocessing. We considered each star particle as a single stellar population with the age, metallicity, and mass assigned to it by the simulation. Stars with metallicities less than  $Z = .0005$  were assigned that minimum value. GRASIL models the distribution of molecular clouds and dust based on the structural parameters of a galaxy disk and bulge. The quoted magnitudes in Table 5 are the average of different viewing angles.

Figures 12 and 13 show our galaxy models overplotted on TF and baryonic TF data from Giovanelli (2005, private communication) and McGaugh (2005), respectively. The opposite residuals for DWF1 and MW1 from the average TF relation (continuous line in

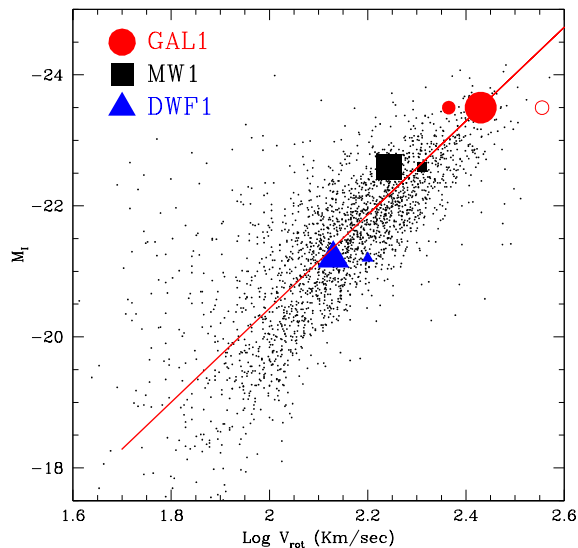


**Figure 12.** The Tully Fisher relation using the data compilation from Giovanelli 2005 (private communication) and a fit to Giovanelli et al. (1997). Solid triangle: DWF1, Solid Square: MW1, Solid Dot: GAL1. Bigger dots shows  $V_{rot}$  measured at  $3.5R_d$ . Smaller dots shows the effect of measuring  $V_{rot}$  at  $2.2R_d$ . The small open dot uses  $V_{rot}$  measured from GAL1 cold gas component

Fig.11) correlate well with their halo spins: lower than average for DWF1 and higher for MW1. As GAL1 dynamical tracers are slightly decoupled (see §5.2), its location on the TF relations somewhat depends on the tracers chosen (old or young stars for the disk scale length, stars or cold gas as tracer of the velocity field). As GAL1’s stellar mass is larger than  $10^{11} M_{\odot}$  it is a likely candidate for an early spiral or even an S0. We speculate that another type of feedback, possibly from an active QSO at the bulge center (Di Matteo et al. 2005; Hopkins et al. 2005), would decrease star formation in the center and lower the central gas density, reducing the relative weight of the central baryonic concentration.

Improvements in matching the Tully Fisher and in conserving the angular momentum content of disks have been consistently reported in the literature as the robustness of simulations and the detail of physical modelling has continued to improve (Sommer-Larsen et al. 2003; Abadi et al. 2003; Governato et al. 2004; Robertson et al. 2004). As we show in §8 our simulations have a softening of the order of only 20% of the disk scale lengths and give robust and likely converging results at scales corresponding to the typical scale length of stellar disks. We verified that our match with the TF relations is not due to  $V_{rot} \ll$

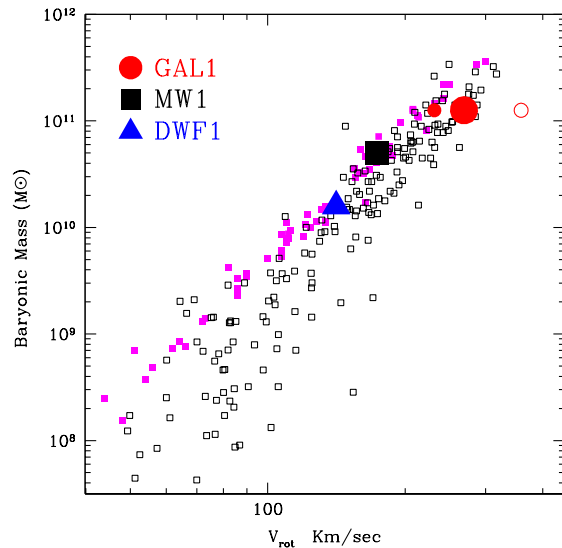


**Figure 13.** The Baryonic Tully Fisher relation. Squares show data points from (McGaugh 2005).  $V_{rot}$  is measured at  $3.5R_d$  (as in the observational sample) for each of the three galaxies. The two smaller points for the GAL1 run show the effect of measuring  $V_{rot}$  at  $2.2 R_d$  using stars and the cold gas component, as shown in Figure 12.

$V_c$ , i.e. the disks are not dynamically “hot” within a few disk scale lengths and gas and young stars trace very closely the underlying potential. We verified that runs with no feedback produce galaxies slightly redder, but only in the B band and only for DWF1 where the effect is 0.3 mag with  $\epsilon_{SN} = 0.4$  and 0.5 mag for  $\epsilon_{SN} = 0.6$ . For more massive galaxies and/or redder bands the effect is only 0.1 - 0.05 mag as the effect of feedback is smaller and star formation happen mostly at higher redshifts. This small color shift is not sufficient to explain the shift from the I band TF measured in some previous simulations.

## 7 FEEDBACK AND THE STAR FORMATION HISTORIES OF GALAXIES

Not only does feedback affect the structure and stability of disks, as discussed in §5.1 and §5.2 respectively, but we also expect it to shape their star formation histories. The isolated test simulations of §2 hinted at this effect, and in this Section we explore the effect of feedback on the star formation histories of DWF1, MW1, and GAL1. The SFHs of bulge and disk stars in these three runs are shown in Figure 14. The plot shows that the peak of star formation is delayed in less massive halos, as expected if feedback has a more pronounced effect in



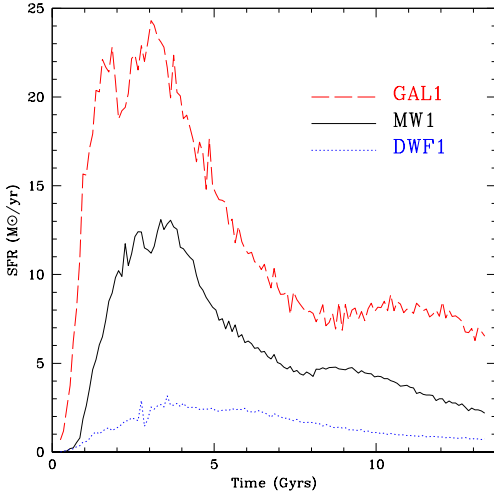


**Figure 14.** Star formation histories of DWF1, MW1, and GAL1, including all stars within 4 disk radial and vertical scale heights.  $\epsilon\text{SN}=0.4$  and UV field on for all runs. Solid black: MW1, long dashed: GAL1, dotted: DWF1.

galaxies with shallower potential wells (Maller & Dekel 2002). To understand this result, consider the natural property of CDM models that star formation at high redshift happens in a number of progenitors that eventually coalesce to form a present day galaxy. We used the DWF1 simulation to verify that increasing feedback limits the efficiency of star formation in progenitor halos with  $V_c < 30\text{-}50$  km/sec and delays it until small subhalos merge into halos with a sufficiently deep potential well (see also Neistein et al. (2006)).

To illustrate the crucial effect of feedback on the SFH of DWF1, Figure 15 compares its SFH in the absence of feedback and with  $\epsilon\text{SN} = 0.6$ , the strongest feedback adopted in our study. Early star formation is significantly reduced in the case of feedback, and we no longer see the initial strong starbursts evident in the run with no feedback. Lowering the efficiency of star formation during mergers preserves a large quantity of cold gas that rapidly settled in rotationally supported disks. The run with feedback has a present day SFR almost ten times higher than that without. The SFR in the run with feedback is far too low to match observations.

The  $z = 0$  star formation rates of DWF1, as well as of the other two galaxies, are quite similar to those observed in galaxies with the same stellar mass. Figure 16 shows the  $z = 0$  star formation rates of our simulated galaxies overlotted with those measured for SDSS galaxies in a wide mass range (Brinchmann et al. 2004). Two low mass field galaxies outside the virial radius of galaxy MW1 (but within the high resolution region) have also been included to show a fair agree-

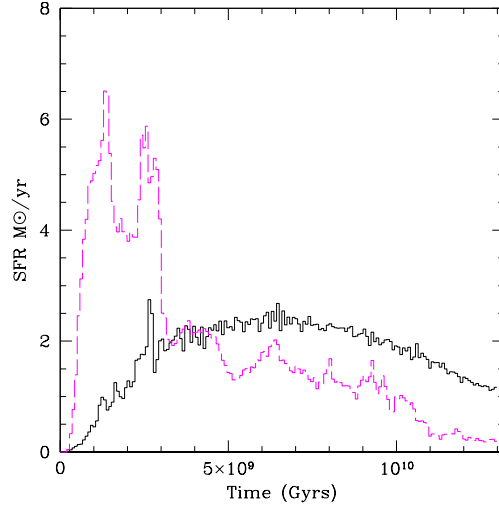


**Figure 15.** Galaxy DWF1: SFH including all stars within  $4 R_z$  and  $R_d$  from the disk plane for two runs. Solid line:  $\epsilon\text{SN}=0.6$ , long dashed: no feedback, no UV. The addition of feedback smooths out the SF peaks otherwise present at high redshift and during the last major merger event at  $z=2.3$ . Feedback delays the conversion of gas into stars until gas accumulates and cools in the potential well of the main progenitor.

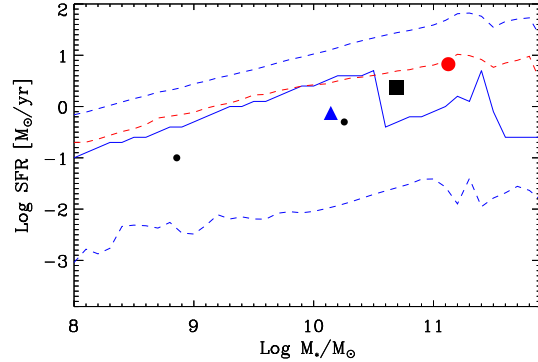


**Figure 16.** Present day star formation rate vs galaxy stellar mass for both simulated and observed galaxies. Triangle: DWF1, Square: MW1. Solid Circle: GAL1. The two smaller dots are field galaxies in the high resolution region of our simulations. The continuous line is the average SFR for the SDSS sample described in Brinchmann et al. (2004). The central dashed line is the median value. The upper and lower dashed lines include data three sigma from the mean of the observational sample



ment between our theoretical model and observational data over more than two orders of magnitude in stellar mass.

Our galaxy models run with SN feedback also reproduce the observed “downsizing” of field galaxies (Cowie et al. 1996; MacArthur et al. 2004): galaxies with a less massive stellar component are also younger. Figure 17 shows that the inclusion of feedback and its differential effects at different galaxy masses naturally reproduces the observed trend: more massive galaxies also have older stellar populations. This trend disappears when runs with no feedback are considered (open circles) and average stellar ages correspond to the time of collapse of the first protogalaxies. As SN feedback removes baryons and delays star formation in smaller halos, it has a stronger effect in less massive galaxies that formed from even less massive progenitors at high redshift. Gas must collect inside a sufficiently deep potential well before it is able to cool efficiently. More massive galaxies are formed from the merging of more massive progenitors, that were able to form stars already at high redshift. While CDM forms structure from the bottom up, the introduction of feedback reverses the trend for stellar populations.

Recently, Bell & de Jong (2001) and Conselice et al. (2005) used observations of spiral galaxies to measure the stellar mass associated with galaxies of different rotational velocities and halo mass. A comparison of our simulations with data in Conselice et al. (2005) and the best fit to Bell & de Jong (2001) is plotted in Fig.18 and shows that our models form the right amount of stars in their bulge and disk components. We also verified that MW1 contains  $4 \times 10^{10} M_{\odot}$  of dark matter within 8.5 kpc, again in good agreement with estimates for the Milky Way (Eke et al. 2001). These results confirm that our modelling of SF and feedback created galaxies with the right amount of stars for their halo mass.

## 8 RESOLUTION TESTS: THE CENTRAL MASS PROFILE OF GALAXIES AND THE LUMINOSITY FUNCTION OF SATELLITES.

In this section, we show that our results are robust to resolution effects. To do this, we have performed one additional simulation (MW1hr) to test if our results have converged as resolution is further increased. A more complete study on how resolution affects the formation of disks and the general properties of galaxies is highly needed but beyond the scope of this paper. MW1hr uses the same initial conditions as the MW1 runs, but uses eight times as many particles within the high resolution region.  $\epsilon_{\text{SN}} = 0.6$  (as for run MW1g4) was used. Force resolution is improved by a factor of two to 0.3 kpc. Additional waves in the initial perturbations spectrum are

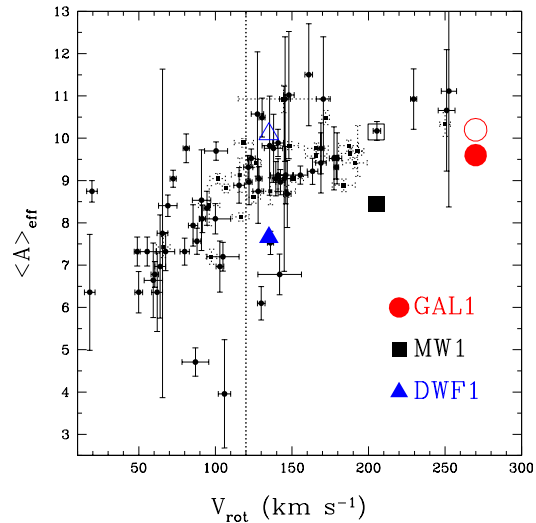


**Figure 17.** Mass weighted average age of stellar populations vs galaxy stellar mass. Small dots with error bars: from MacArthur et al. (2004). Solid large dots: simulations with  $\epsilon_{\text{SN}} = 0.4$ . Open dots: simulations with no feedback or UV.  $V_{\text{rot}}$  is measured at 3.5 disk scale lengths.

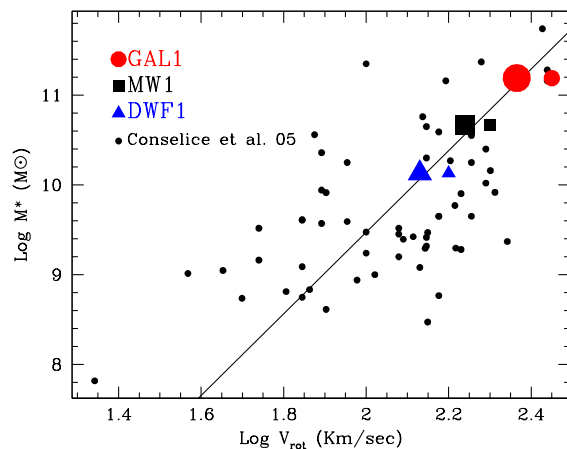


**Figure 18.** Total stellar mass vs. rotational velocity. Solid small dots are data from Conselice et al. (2005). Large dots: simulations measured at  $3.5 R_d$ . Small points: simulations measured at  $2.2 R_d$ . The straight line is a fit from Bell & de Jong (2001).

consistently added. With a dark matter particle mass of only  $7.6 \times 10^5 M_\odot$  and star particle mass of  $3 \times 10^4 M_\odot$  this simulation has one of the highest resolutions for a Milky Way sized galaxy in a cosmological context to date. Due to its high computational cost we carried this simulation only to  $z = 0.5$ , using several tens of thousands of CPU hours. Figure 19 compares the circular velocity  $V_c$  of MW1g4 and MW1hr (again defined as  $\sqrt{M(r < R)/R}$ ) for the DM, baryonic and stellar components, while Figure 20 compares the V-band satellites luminosity function (again at  $z=0.5$ ).

Figure 19 shows that at the resolution of our standard runs the total mass profile and the quantity of stars have converged at radii corresponding to a couple of disk scale lengths.  $V_{rot}$  measured at  $3.5R_D$  (and used in Figures 12, 13, 17 and 18) is thus robust to resolution effects, at the resolution of our standard runs. Test runs in a cosmological context resolution (Governato et al in prep.) show a systematic increase in  $V_c$  and a decrease of stellar  $R_D$  as resolution becomes increasingly worse. This result likely explains why our simulations match the normalization of the TF relation. However at smaller radii (only 3-4 times the gravitational softening) our standard run MW1g4 shows a much larger central mass than MW1hr. This unphysical mass concentration significantly raises the  $V_c$  such that it peaks at over 300km/sec. Because the standard and high resolution runs adopted identical feedback and SF parameters, this result shows that resolution plays an important role in the central region of galaxies. In DM-only simulations, low resolution artificially lowers central DM densities. In contrast with DM only simulations, low resolution and lack of feedback in SPH simulations causes baryons to become more centrally concentrated due to partially artificial angular momentum loss. As resolution is increased, reduced artificial angular momentum loss by both the stellar and gaseous component allow SN feedback to be more effective and to reduce the central baryon concentration. Worse resolution and possibly weaker feedback would have overestimated the amount of baryons within  $2.2 R_d$ . As the force resolution is increased the disk bar instability in the disk of MW1hr starts earlier ( $z \sim 2$ ) and is more pronounced than in the MW1g4 simulation, confirming studies by Kaufmann & Mayer (2006). At this high resolution the fraction of cold baryons is 40% higher, and the mass in stars is only 5% lower. We also begin to resolve the thermal instabilities predicted by Maller & Bullock (2004) and recently detected in simulations of isolated galaxies (Kaufmann et al. 2004). It is encouraging that the satellite V-band luminosity function (Fig.20) remains substantially unaltered as resolution is increased, although a few more satellites as faint as  $M_V = -8$  are now resolved. This supports results from S06 that our adopted SF+SN algorithm is relatively insensitive to resolution.

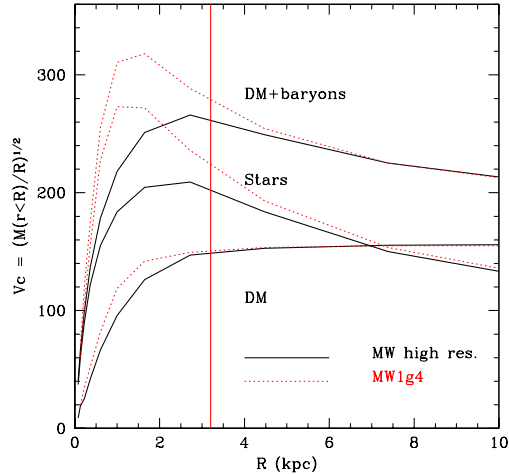


**Figure 19.** Resolution tests: The circular velocity  $V_c = \sqrt{M(< R)/R}$  for run MW1hr (solid) and MW1g4 (dots). The mass distribution converges at radii larger than  $r > 2.2 R_d$  (vertical line). The high resolution simulation contains significantly less baryons within a few times  $\epsilon$

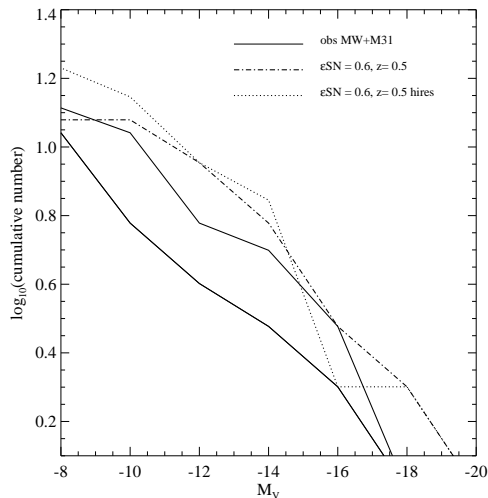


**Figure 20.** Resolution tests: The V – band luminosity function of the satellites system of MW1g4 (dashed) and its high resolution version (dotted) at  $z = 0.5$  compared with the Milky Way and Andromeda (solid lines).

## 9 CONCLUSIONS

We have presented a new set of simulations of the formation of disk dominated galaxies in a full  $\Lambda$ CDM cosmological context carried to the present time. These simulations included a simple but physically motivated recipe for star formation. We used isolated galaxy models to calibrate the free parameters of our star formation/feedback scheme to reproduce several important properties of the stellar and ISM components of local disk galaxies over a range of masses. We then used this SF/feedback algorithm in cosmological simulations with no further adjustment.

We simulated three different halos in a cosmological context, with masses typical of those associated with disk galaxies. These cosmological simulations have a very high number of resolution elements within the virial radius of the simulated galaxies ( $\sim 1.5 \cdot 10^5$  for each of the DM and gas components and a few hundred thousand star particles), allowing us to resolve individual satellites down to  $V_c \sim 20\%$  of the parent galaxy. A rotation dominated stellar disk galaxy with a significant exponential component naturally forms within each of these halos. Our MW1 simulation provides a good example of how the stellar disk can form shortly after a major merger event, due to the large amount of orbital angular momentum transferred to the gas component during the merger event. Our three simulated galaxies (DWF1, MW1, GAL1) share the size, stellar mass, colors and current SFR typical of a low mass galaxy, of a Milky Way like galaxy and a massive early type spiral, respectively.

One of our most significant results is that the simulated galaxies fall on the TF and baryonic TF relations. This match is possible in part due to the high resolution of the simulations: Resolution is crucial to avoid artificially losing the angular momentum gained this way (Governato et al. 2004; Kaufmann & Mayer 2006). At our resolution, rotation curves have been resolved down to a fraction of the stellar disk scale lengths and (measured at  $3.5 R_d$ ) range from 135 to 270 km/sec in amplitude. The MW sized galaxy contains an amount of DM within the solar radius well in agreement with observational constraints. The simulated galaxies also reproduced the observed 'anti-hierarchical' trend of stellar populations: smaller galaxies have younger stellar populations. As feedback delays star formation in protogalaxies a larger reservoir of gas remains available to form disks until the bulk of the mass of galaxy is assembled, typically between redshift 3 and 1. Feedback and the cosmic UV field also drastically reduce the number of galaxy satellites containing a significant stellar population.

We have complemented our standard runs with a high resolution test run of our MW sized halo. This run has an unprecedented number of particles: several mil-

lion within  $R_{vir}$ . We used it to test the convergence of results in our standard runs. At our highest resolution the main galaxy is significantly less centrally concentrated, reducing its bulge mass and its peak velocity considerably. While stellar bulges are likely still unresolved in our standard runs, our tests and estimates from previous works suggest that the mass distribution and the rotation velocity of the cold gas and young stellar components have converged at the scales of a few kpc. Such a high resolution coupled with a physically motivated description of feedback explains why our models do indeed fall onto the TF relations.

These simulations and those published in the recent literature show that some significant progress has been done toward understanding galaxy formation in the context of a  $\Lambda$ CDM concordance cosmology. However, areas where progress needs to be made: (i) A larger range of initial conditions needs to be explored to understand the role played by halo spin and merging history on the morphology and colors of galaxies; (ii) Our resolution test shows that the inner mass distribution of the galaxies, including the bulge, is still poorly resolved by our standard runs and that possibly several million resolution elements per galaxy are needed to approach convergence; (iii) Satellites are still too bright compared to those orbiting our Milky Way. While cosmic variance likely played a role (the largest satellites accreted by the MW1 system is more massive than the LMC), one obvious possibility to create fainter satellites would be to increase the efficiency of SN feedback, but that needs to be carefully calibrated with the other constraints. Two intriguing possibilities that we plan to explore in future works are the increased feedback and UV field due to massive POPIII stars (Choudhury & Ferrara 2005) and the local proximity effect that star formation from the main galaxy might have on the nearby dwarfs (Gnedin 2000). Overall, the possibility of obtaining a good match to the observed satellite LF seems within reach of future simulations.

## ACKNOWLEDGMENTS

FG would like to thank A. Dekel, E. D'Onghia, T. Kaufmann, J. Silk & M. Steinmetz, for helpful conversations during this project. We thank J. Brinchmann, C. Conzelmann, S. McGaugh, L. MacArthur and R. Giovanelli for sharing their data with us. Support for this work, part of the Spitzer Space Telescope Theoretical Research Program, was provided by NASA through a contract issued by the Jet Propulsion Laboratory, California Institute of Technology under a contract with NASA. FG was a Brooks Fellow during the initial stages of this project and was supported in part by NSF grants AST-0098557 and AST-61-3931. TRQ acknowledges support from NSF grant AST-0098557 and NSF grant PHY-0205413. Most simulations were run at the Arctic Re-

gion Supercomputing Center and on a local SGI multi-CPU machine.

## REFERENCES

- Abadi M. G., Navarro J. F., Steinmetz M., Eke V. R., 2003, *ApJ*, 591, 499
- Balogh M. L., Pearce F. R., Bower R. G., Kay S. T., 2001, *MNRAS*, 326, 1228
- Balsara D. S., 1997, in *ASP Conf. Ser. 123: Computational Astrophysics; 12th Kingston Meeting: Modern Schemes for Solving Hyperbolic Conservation Laws of Interest in Computational Astrophysics on Parallel Machines*. p. 274
- Bardeen J. M., Bond J. R., Kaiser N., Szalay A. S., 1986, *ApJ*, 304, 15
- Barnes J. E., Hernquist L., 1996, *ApJ*, 471, 115
- Baugh C. M., Cole S., Frenk C. S., 1996, *MNRAS*, 283, 1361
- Bell E. F., de Jong R. S., 2001, *ApJ*, 550, 212
- Benson A. J., Frenk C. S., Lacey C. G., Baugh C. M., Cole S., 2002, *MNRAS*, 333, 177
- Benz W., 1990, in *Numerical Modelling of Nonlinear Stellar Pulsations Problems and Prospects Smooth Particle Hydrodynamics - a Review*. pp 269–+
- Binney J., Gerhard O., Silk J., 2001, *MNRAS*, 321, 471
- Bizyaev D., Mitronova S., 2002, *A&A*, 389, 795
- Blanton M. R. e. a., 2003, *ApJ*, 594, 186
- Blumenthal G. R., Faber S. M., Primack J. R., Rees M. J., 1984, *Nature*, 311, 517
- Brinchmann J., Charlot S., White S. D. M., Tremonti C., Kauffmann G., Heckman T., Brinkmann J., 2004, *MNRAS*, 351, 1151
- Broeils A. H., Rhee M.-H., 1997, *A&A*, 324, 877
- Brook C. B., Kawata D., Gibson B. K., Freeman K. C., 2004, *ApJ*, 612, 894
- Bundy K., Ellis R., Conselice C., 2005, *astro-ph/0502204*
- Catinella B., Giovanelli R., Haynes M. P., 2006, *ApJ*, 640, 751
- Cen R., Ostriker J. P., 1999, *ApJ*, 514, 1
- Choudhury T. R., Ferrara A., 2005, *MNRAS*, 361, 577
- Cole S., Lacey C. G., Baugh C. M., Frenk C. S., 2000, *MNRAS*, 319, 168
- Conselice C. J., Bundy K., Ellis R. S., Brinchmann J., Vogt N. P., Phillips A. C., 2005, *ApJ*, 628, 160
- Cowie L. L., Songaila A., Hu E. M., Cohen J. G., 1996, *AJ*, 112, 839
- Davis M., Efstathiou G., Frenk C. S., White S. D. M., 1985, *ApJ*, 292, 371
- Debattista V. P., Carollo C. M., Mayer L., Moore B., 2004, *ApJ*, 604, L93
- Debattista V. P., Mayer L., Carollo C. M., Moore B., Wadsley J., Quinn T., 2005, *astro-ph/0509310*
- Dekel A., Woo J., 2003, *MNRAS*, 344, 1131
- Di Matteo T., Springel V., Hernquist L., 2005, *Nature*, 433, 604
- Diemand J., Moore B., Stadel J., Kazantzidis S., 2004, *MNRAS*, 348, 977
- D’Onghia E. e. a., 2006, *astro-ph/0602005*
- Efstathiou G., 2000, *MNRAS*, 317, 697
- Efstathiou G., Lake G., Negroponte J., 1982, *MNRAS*, 199, 1069
- Eke V., Efstathiou G., Wright L., 2000, *MNRAS*, 315, L18
- Eke V. R., Navarro J. F., Steinmetz M., 2001, *ApJ*, 554, 114
- Elmegreen B. G., Elmegreen D. M., Vollbach D. R., Foster E. R., Ferguson T. E., 2005, *ApJ*, 634, 101
- Evrard A. E., 1988, *MNRAS*, 235, 911
- Fall S. M., 1983, in *IAU Symp. 100: Internal Kinematics and Dynamics of Galaxies Galaxy formation - Some comparisons between theory and observation*. pp 391–398
- Fall S. M., Efstathiou G., 1980, *MNRAS*, 193, 189
- Ferrara A., 2002, in *ASP Conf. Ser. 285: Modes of Star Formation and the Origin of Field Populations Stellar Feedback, Dark Matter and Dwarf Evolution (Review)*
- Ferreras I., Silk J., Böhm A., Ziegler B., 2004, *MNRAS*, 355, 64
- Florido E., Battaner E., Gujarro A., Garzón F., Jiménez-Vicente J., 2001, *A&A*, 378, 82
- Frenk C. S., White S. D. M., Efstathiou G., Davis M., 1985, *Nature*, 317, 595
- Gallazzi A., Charlot S., Brinchmann J., White S. D. M., Tremonti C. A., 2005, *MNRAS*, 362, 41
- Gardner J. P., 2001, *ApJ*, 557, 616
- Gerritsen J. P. E., 1997, Ph.D. Thesis
- Giovanelli R., Haynes M. P., Herter T., Vogt N. P., da Costa L. N., Freudling W., Salzer J. J., Wegner G., 1997, *AJ*, 113, 53
- Gnedin N. Y., 2000, *ApJ*, 535, 530
- Governato F., Mayer L., Wadsley J., Gardner J. P., Willman B., Hayashi E., Quinn T., Stadel J., Lake G., 2004, *ApJ*, 607, 688
- Governato F., Moore B., Cen R., Stadel J., Lake G., Quinn T., 1997, *New Astronomy*, 2, 91
- Granato G. L., De Zotti G., Silva L., Bressan A., Danese L., 2004, *ApJ*, 600, 580
- Haardt F., Madau P., 1996, *ApJ*, 461, 20
- Haehnelt M. G., Steinmetz M., Rauch M., 1998, *ApJ*, 495, 647
- Hopkins P. F., Hernquist L., Cox T. J., Di Matteo T., Martini P., Robertson B., Springel V., 2005, *ApJ*, 630, 705
- Katz N., 1992, *ApJ*, 391, 502
- Katz N., Weinberg D. H., Hernquist L., 1996, *ApJS*, 105, 19
- Kaufmann T., Mayer L., Moore B., Stadel J., Wadsley J., 2004, *Baryons in Dark Matter Halos*

- Kaufmann T., Mayer L. e. a., 2006, ArXiv Astrophysics e-prints
- Kawata D., Arimoto N., Cen R., Gibson B., 2005, astro-ph/0509402
- Kennicutt R. C., 1998, ApJ, 498, 541
- Klypin A., Kravtsov A. V., Valenzuela O., Prada F., 1999, ApJ, 522, 82
- Klypin A., Zhao H., Somerville R. S., 2002, ApJ, 573, 597
- Kormendy J., Kennicutt R. C., 2004, 42, 603
- Kravtsov A. V., Gnedin O. Y., 2005, ApJ, 623, 650
- Kravtsov A. V., Gnedin O. Y., Klypin A. A., 2004, ApJ, 609, 482
- Krumholz M., McKee C., 2005, astro-ph/0505177
- Lake G., Carlberg R. G., 1988, AJ, 96, 1587
- Li Y., Mo H., van den Bosch F., 2005
- Mac Low M., Ferrara A., 1999, ApJ, 513, 142
- MacArthur L. A., Courteau S., Bell E., Holtzman J. A., 2004, ApJS, 152, 175
- Macciò A. V., Governato F., Horellou C., 2005, MNRAS, 359, 941
- Maller A. H., Bullock J. S., 2004, MNRAS, 355, 694
- Maller A. H., Dekel A., 2002, MNRAS, 335, 487
- Martin C. L., 1999, ApJ, 513, 156
- Martin D. C., Fanson J., Schiminovich D. e. a., 2005, ApJ, 619, L1
- Mateo M. L., 1998, 36, 435
- Mayer L., Moore B., 2004, MNRAS, 354, 477
- Mayer L., Wadsley J., 2004, MNRAS, 347, 277
- McGaugh S. S., 2005, ApJ, 632, 859
- McGaugh S. S., Schombert J. M., Bothun G. D., de Blok W. J. G., 2000, ApJ, 533, L99
- McKee C. F., Ostriker J. P., 1977, ApJ, 218, 148
- Mo H. J., Miralda-Escude J., 1996, ApJ, 469, 589
- Monaco P., 2004, MNRAS, 352, 181
- Monaghan J. J., 1992, 30, 543
- Moore B., Ghigna S., Governato F., Lake G., Quinn T., Stadel J., Tozzi P., 1999, ApJ, 524, L19
- Navarro J. F., Steinmetz M., 1997, ApJ, 478, 13
- Navarro J. F., Steinmetz M., 2000, ApJ, 538, 477
- Navarro J. F., White S. D. M., 1994, MNRAS, 267, 401
- Neistein E., van den Bosch F. C., Dekel A., 2006, MNRAS, 372, 933
- Nordström B., Mayor M., Andersen J., Holmberg J., Pont F., Jørgensen B. R., Olsen E. H., Udry S., Mowlavi N., 2004, A&A, 418, 989
- Okamoto T., Eke V. R., Frenk C. S., Jenkins A., 2005, MNRAS, 363, 1299
- Ostriker J. P., McKee C. F., 1988, Reviews of Modern Physics, 60, 1
- Peebles P. J., Ratra B., 2003, Reviews of Modern Physics, 75, 559
- Peebles P. J. E., 1969, ApJ, 155, 393
- Pizzella A., Corsini E. M., Vega Beltrán J. C., Bertola F., 2004, A&A, 424, 447
- Pohlen M., Balcells M., Lütticke R., Dettmar R.-J., 2004, A&A, 422, 465
- Pohlen M., Trujillo I., 2005
- Quinn T., Katz N., Efstathiou G., 1996, MNRAS, 278, L49
- Raiteri C. M., Villata M., Navarro J. F., 1996, A&A, 315, 105
- Robertson B., Yoshida N., Springel V., Hernquist L., 2004, ApJ, 606, 32
- Ryder S. D., Dopita M. A., 1994, ApJ, 430, 142
- Seth A. C., Dalcanton J. J., de Jong R. S., 2005, AJ, 129, 1331
- Shen S., Mo H. J., White S. D. M., Blanton M. R., Kauffmann G., Voges W., Brinkmann J., Csabai I., 2003, MNRAS, 343, 978
- Silk J., 2001, MNRAS, 324, 313
- Silva L., Granato G. L., Bressan A., Danese L., 1998, ApJ, 509, 103
- Slyz A. D., Devriendt J. E. G., Bryan G., Silk J., 2005, MNRAS, 356, 737
- Sommer-Larsen J., Götz M., Portinari L., 2003, ApJ, 596, 47
- Spergel D. N., Verde L., Peiris H. V., Komatsu E., Nolte M. R., Bennett C. L., Halpern M., Hinshaw G., Jarosik N., Kogut A., Limon M., Meyer S. S., Page L., Tucker G. S., Weiland J. L., Wollack E., Wright E. L., 2003, ApJS, 148, 175
- Springel V., 2000, MNRAS, 312, 859
- Springel V., Hernquist L., 2002, MNRAS, 333, 649
- Springel V., Hernquist L., 2005, ApJ, 622, L9
- Steinmetz M., Navarro J. F., 2002, New Astronomy, 7, 155
- Stinson G., Seth A., Katz N., Governato F., Wadsley J., Quinn T., 2006, astro-ph/0602350
- Tasker E. J., Bryan G., 2005
- Thacker R. J., Couchman H. M. P., 2000, ApJ, 545, 728
- Tittley E. R., Pearce F. R., Couchman H. M. P., 2001, ApJ, 561, 69
- Toomre A., Toomre J., 1972, ApJ, 178, 623
- Trujillo I., et al., 2005, astro-ph/0504255
- Valenzuela O., Klypin A., 2003, MNRAS, 345, 406
- Wada K., Norman C. A., 2001, ApJ, 547, 172
- Wadsley J. W., Stadel J., Quinn T., 2004, New Astronomy, 9, 137
- West A. A., Garcia-Appadoo D. A., Dalcanton J. J., Disney M. J., 2005, in AIP Conf. Proc. 761: The Spectral Energy Distributions of Gas-Rich Galaxies: Confronting Models with Data HI Selected Galaxies in the SDSS. pp 409+
- White S. D. M., Frenk C. S., 1991, ApJ, 379, 52
- White S. D. M., Rees M. J., 1978, MNRAS, 183, 341
- Willman B., Governato F., Dalcanton J. J., Reed D., Quinn T., 2004, MNRAS, 353, 639
- Yepes G., Kates R., Khokhlov A., Klypin A., 1997, MNRAS, 284, 235

Yoachim P., Dalcanton J. J., 2005, ApJ, 624, 701  
Yoachim P., Dalcanton J. J., 2006, AJ, 131, 226